X-ray crystal structure analysis of reduced and ligand-bound nitric oxide reductase from *Pseudomonas aeruginosa*

Nozomi SATO

2014

CONTENTS

Chapter 1

General introduction

Nitric oxide reductase (NOR) is an iron-containing enzyme located at cellular membrane, which catalyzes the reduction of nitric oxide (NO) to nitrous oxide (N_2O), a major greenhouse gas. The N_2O potential of contributeion to global warming is 200-300 times greater than that of CO_2 (Watmough *et al.*, 2009). The largest emission of N_2O on the earth is bacterial breakdown of nitrogen compounds derived from artificial fertilizers that contain soluble nitrate (NO_3^-) and nitrite (NO_2^-) as nitrogen sources. Some bacteria reduce NO_3^- to dinitrogen via NO_2^-, NO and N_2O. This process, so-called denitrification ($NO_3^- \rightarrow NO_2^- \rightarrow NO \rightarrow N_2O \rightarrow N_2$), is a form of bacterial anaerobic respiration, in which NO_3^- is used as a terminal electron acceptor to produce bio-available energy, ATP, contrary to aerobic respiration utilizing molecular oxygen. NOR is one of the enzymes involved in the denitrification process and directly contributes to biological N_2O generation.

From the similarity of the amino acid sequences, NOR belongs to the superfamily of heme-copper oxidases, which contains aerobic respiratory enzymes such as cytochrome *c* oxidize (CCO) (Saraste & Castresana, 1994). Indeed, all His ligands for the active site metals are conserved in NORs and

Coos. It was, therefore, suggested that NOR and CCO are evolutionary related to each other and share the same progenitor protein (Ducluzeau *et al.*, 2009; Pereira *et al.*, 2001; Saraste & Castresana, 1994; Sousa *et al.*, 2012). However, the catalytic binuclear center of NOR consists of heme (heme b_3) and non-heme iron (Fe_B), which differs from heme and Cu (Cu_B) binuclear active center in CCO (Fig. 1). Fe_B in NOR is in the original bipyramidal geometry with three His and one Glu ligands (Fig. 1A), although three His ligands for Cu_B creates distorted planar geometry in CCO (Fig. 1B). Furthermore, a functionally important His-Tyr covalent linkage common in the binuclear center of CCO is absent in NOR. These structural characteristics are supposed to be crucial for the respective function of the respiratory enzymes; NOR catalyzes NO reduction ($2NO + 2H^+ + 2e^- \rightarrow N_2O + H_2O$), while CCO catalyzes four electron reduction of oxygen molecule ($O_2 + 4H^+ + 4e^- \rightarrow 2H_2O$). Alternative functional difference between NOR and CCO is that NOR shows no proton pumping ability, which is an essential function for CCO and coupled with the catalytic O_2 reduction reaction to generate electrochemical gradient across the membrane. On the basis of the high resolution structural analysis for Coos, several proton transfer pathways designated as D-, K- and H-pathways were proposed (Ferguson-Miller *et al.*, 2012; Matsumoto *et al.*, 2012; Qin *et al.*, 2009; Tsukihara *et al.*, 2003; Yoshikawa *et al.*, 1998; Yoshikawa *et al.*, 2006). Although the structure of NOR, especially the transmembrane region, is closely similar to CCO, any of

the D-, K- and H-proton pathways was not observed in the structure of NOR (Hino *et al.*, 2010). This structural observation is consistent with the fact that NOR does not pump protons (Flock *et al.*, 2008). Thus, the structural and functional studies on NOR should help us understanding the molecular evolution of the respiratory enzymes.

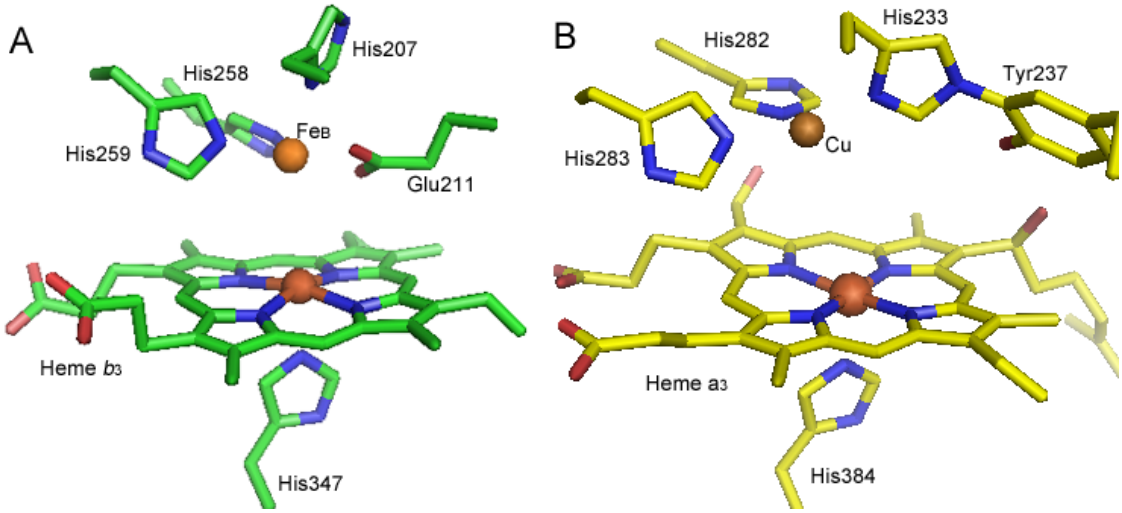

Figure 1. Structure of the binuclear center of NOR and CCO. Panel (A) shows non-heme iron(Fe_B) is coordinated by Glu211, His207, His258 and His259 in the original bipyramidal geometry in cNOR from *P. aeruginosa*. Panel (B) shows Cu is coordinated by His233, His282 and His283 in the distorted planar geometry in CCO.

The NOR reaction is also an attractive subject for fundamental chemistry, because it involves N-O bond cleavage and N-N bond formation. So far, several catalytic reaction mechanisms have been suggested as shown

in Scheme 1 on the basis of the chemical, spectroscopic and theoretical studies of NOR (Blomberg & Siegbahn, 2012; Collman *et al.*, 2008; Kumita *et al.*, 2004; Moenne-Loccoz, 2007; Timoteo *et al.*, 2011; Yi *et al.*, 2012). In a previous study, it was suggested that only a cis:b_3 mechanism was energetically feasible, and the suggested alternative trans mechanism has to be rejected as energetically unfavorable (Blomberg & Siegbahn, 2012). Despite the accumulation of the impressive body of knowledge on the NO reduction reaction by NOR, the detailed mechanism for the NOR-catalyzed reaction is still unclear owing to the paucity of the structural information.

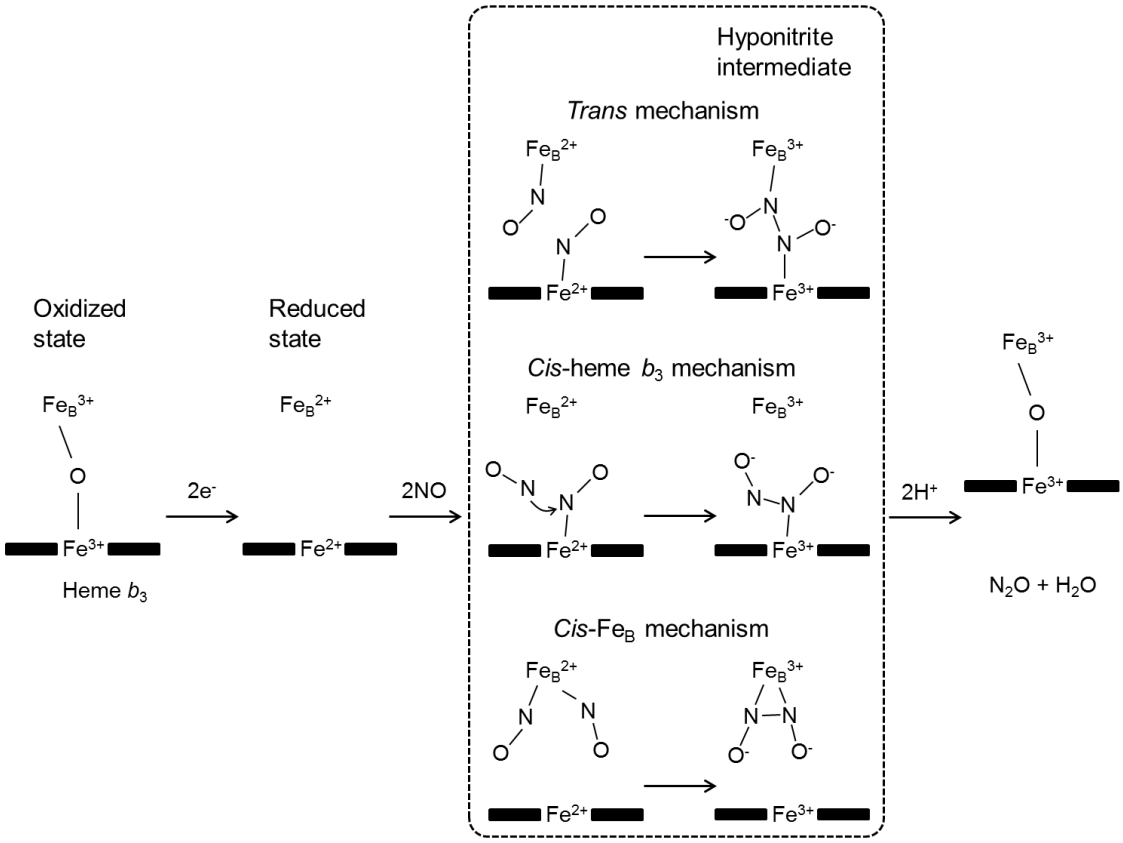

Scheme 1. Presumed NO reduction mechanism in NOR.

Three different classes of NOR have been identified in bacteria and archaea. First type of NOR, which is called cytochrome *c*-dependent NOR (cNOR), is only observed in denitrifying bacteria, and this enzyme is composed of Nor and Norco subunits. cNOR uses proteinous electron donors such as cytochrome *c* for the catalytic reaction. The second enzyme, as quoin-dependent NOR (qNOR), is a single subunit enzyme that is observed in non-denitrifying pathogenic bacteria as well as denitrifying bacteria and archaea (Ducluzeau *et al.*, 2009). The physiological role of qNOR of pathogenic bacteria is to detoxify NO produced by the immune system of the host (Stevanin *et al.*, 2005). qCu_ANOR, which was isolated from denitrifying *Bacillus azotoformance* and has a di-copper site at the hydrophilic domain (Suharti *et al.*, 2001), is third type of NOR. Except for the fact that both cytochrome *c* and quoin can donate electrons to qCu_ANOR, little is known about this enzyme. Of these NOR enzymes, cNOR is most extensively studied in terms of the structure and function (Blomberg & Siegbahn, 2012; Kumita *et al.*, 2004; Moenne-Loccoz, 2007; Reimann *et al.*, 2007). The crystal structure of oxidized form of cNOR from *Pseudomonas aeruginosa* was revealed in 2010 (Hino *et al.*, 2010), which enabled us to discuss the structure-function relationship in NOR. However, to understand the mechanism of the NO reducing reaction by NOR, the structures involved in the catalytic reaction cycle, such as reduced and substrate-bound states, need to be characterized. These structural information are also invaluable to

elucidate the structural elements responsible for the respective function of the respiratory enzymes.

In this thesis, to gain insights into the molecular mechanism for the NO reduction reaction by NOR, I focused on cNOR from *P. aeruginosa*. X-ray crystallography is a powerful technique for the investigation of the molecular structure at atomic level. However, since cNOR is a membrane-integrated protein which is generally difficult to crystallize, I need to overcome the difficulty in making crystals of cNOR to achieve the purpose of this thesis. In chapter 2, I tried to establish the method for obtaining high quality of crystals that give diffraction data useful for the structural analyses at the high resolution (~2.5 Å). In addition to the difficulty in preparing the crystals, the presence of two strong scatterers, heme b_3 iron and Fe_B, hampered us to determine the atomic structure of the binuclear center of cNOR, particularly in the ligand-bound form. I therefore developed the comprehensive method for X-ray structural analysis of ligand-bound NOR by using the cyanide (CN) bound form of cNOR in chapter 2. CN can bind to both oxidized and reduced cNOR, like substrate NO, which means that the CN-bound form can be a good model for the substrate-bound form of cNOR. With the method established in chapter 2, I determined the atomic structures of the reduced and several ligand-bound forms of cNOR. From the cNOR structures obtained from this work together with the reported results from CCO, I will discuss the mechanism of the NOR-catalyzed reaction and possible

structural elements responsible for the different reactions in NOR and CCO. Finally, I summarized the conclusion obtained from this thesis and proposed future perspective for the study on NOR in chapter 4.

Chapter 2

Development of purification and crystallization for structural analysis of cyanide-bound form of Nitric oxide reductase from *Pseudomonas aeruginosa.*

SUMMARY

Cytochrome *c*-dependent NOR (cNOR) from *Pseudomonas aeruginosa* is a membrane-integrated protein, which catalyzes N_2O generation via reductive N-N coupling at a heme and non-heme iron binuclear center. The high resolution structure of substrate or substrate analog-bound cNOR, in addition to the oxidized resting state, is necessary to elucidate the catalytic mechanism in NOR. Here, I developed the purification methods of cNOR and the preparation of cyanide-bound state of crystals that diffracts X-ray to a higher resolution. The careful examination of the fractions in the additional action exchange chromatography in the final purification step was important for the preparation of homogeneous protein sample. Use of the micro seeding technique in crystallization improved the reproducibility of crystal formation and the size of the crystals. The resolution of obtained crystals was improved from 2.7 Å to 2.3 Å by using the newly developed method. In the oxidized form of cyanide-bound cNOR, the

electron density map suggested the presence of two cyanide molecules at the binuclear center. The comprehensive crystallographic refinement indicated that the occupancy of cyanide was estimated as 80%. The remaining 20% was modeled as a bridging ox ligand that derives from a resting state. By contrast, the refinement of the structure of cyanide-bound cNOR prepared in chemically reduced condition converged to the model of two cyanide ions in full occupancy. It is likely that the reduction disrupted the oxo-bridge and increased the occupancy of cyanides. These observations suggest that cNOR has an ability to concomitantly bind two diatomic molecules at the active site without large structural changes, and possibly to keep two NO substrates in the confined space, thereby facilitating the reductive N-N coupling. The methods established here are applicable to the structural determination of cNOR in complex with other type of ligands.

INTRODUCTION

Pseudomonas. aeruginosa is a gammaproteobacterium that is present in diverse environments and is a gram-negative aerobic coccobacillus. Although classified as an aerobe, *P. aeruginosa* can achieve anaerobic growth with nitrate as a terminal electron acceptor. Microbial metabolism under the microaerobic conditions is even less well-characterized, however it is known that the ecological fate of different organic compounds varies differently with the availability of oxygen molecule. *P. aeruginosa* is among the organisms most commonly isolated from petroleum-contained soils and ground water and has versatile metabolic capabilities (Ridgway *et al.*, 1990).

P. aeruginosa is a denitrifying bacterium which has an anaerobic respiratory chain reducing nitrate (NO_3^-) to dinitrogen (N_2). Being an active denitrifier, it has been reported that the bacteria grow fast without mucoid under aerobic conditions but turn mucoid and form biofilm matrix under microaerobic or anaerobic conditions in the presence of nitrate (Govan & Deretic, 1996). The anaerobic respiration requires four independent enzymatically catalyzed reactions:

$$NO_3^- + 2e^- + 2H^+ \rightarrow NO_2^- + H_2O$$

$$NO_2^- + e^- + 2H^+ \rightarrow NO + H_2O$$

$$2NO + 2e^- + 2H^+ \rightarrow N_2O + H_2O$$

$$N_2O + 2e^- + 2H^+ \rightarrow N_2 + H_2O$$

The enzymes involved in denitrification are nitrate reductase, nitrite reductase, nitric oxide reductase (NOR), and nitrous oxide reductase. Chemical compounds produced during denitrification have manifold effects on the atmosphere, soils and waters and thus, have both agronomic and environmental impacts. For example, nitrogenous oxides released from soils and waters are in part responsible for depleting the ozone layer above the Antarctic, and in part for the initiation of acid rain and global warming (Ravishankara *et al.*, 2009). Among them, nitrous oxide (N_2O), commonly known as a laughing gas, has received special attention in the last years, because it is a powerful greenhouse gas that can persist for up to 150 years while it is slowly broken down in the atmosphere (Bueno *et al.*, 2012). Although N_2O only accounts for around 0.03% of total greenhouse gas emissions, it has a 300-fold greater potential for global warming effects, based on its radiative capacity compared with that of carbon dioxide, CO_2 (Ravishankara *et al.*, 2009; Richardson *et al.*, 2009). The vast majority of N_2O originates from bacterial denitrification in which the NOR enzyme is responsible for N_2O generation. The mechanism of N_2O generation by NOR is an attractive subject for the environmental scientists.

The physiological importance of NOR is also addressed by the role of NO detoxification in several pathogenic bacteria during the infection. Denitrifying *P. aeruginosa* is also known as a common opportunistic pathogen causing pneumonia, nosocomial bloodstream infections, and

serious lung infection in the cystic fibrosis patients (Ju *et al.*, 2005). *P. aeruginosa* has NOR to decompose nitric oxide (NO), which is an important immune mediator (Wink *et al.*, 2011). The essential role of NOR in *P. aeruginosa* was demonstrated by the fact that growth of the bacteria lacking NOR is strongly inhibited by exogenous NO and these mutant organisms are killed more efficiently than isogenic wild-type controlled by NO-producing RAW 264.7 macrophages (Kakishima *et al.*, 2007). This result suggested that *P. aeruginosa* NOR functions as a detoxifying enzyme in the activated macrophages and contributes to the intracellular survival against the host's defense systems (Kakishima *et al.*, 2007). Thus, it is highly desirable to elucidate the mechanism of NO detoxification by NOR for developing new antibiotics.

Membrane-integrated NOR of *P. aeruginosa* is cytochrome *c*-dependent NOR (cNOR), which consists of NorB and NorC subunits. The molecular mechanism of the NOR-catalyzed reaction has been extensively studied using cNOR through chemical, biochemical, physicochemical and theoretical techniques (Blomberg & Siegbahn, 2012; Collman *et al.*, 2008; Kumita *et al.*, 2004; Moenne-Loccoz, 2007; Timoteo *et al.*, 2011). NOR was the last enzyme whose molecular properties became known among the denitrification enzymes (Heiss *et al.*, 1989). In 2010, the crystal structure of *P. aeruginosa* cNOR in the resting oxidized state was reported (Hino *et al.*, 2010). The structure showed the details of the heme (heme b_3) and non-heme

iron (Fe_B) binuclear active center in the resting sate, and provided insights into the catalytic proton transfer pathway. However, to understand more about the mechanism of the N_2O generation (NO reduction) by NOR, structures included in the reaction cycle need to be characterized.

In this chapter, I aimed at developing new methods for the purification and crystallization of cNOR from *P. aeruginosa* to obtain better quality crystals. By using the method developed here, I obtained crystals of cyanide-bound (a substrate analog bound) cNOR both in the oxidized and reduced states and diffraction data at a resolution of ~2.5 Å. Through the structural analyses of cyanide-bound cNOR, a method for the structural determination of the binuclear active center in which two strong scatters, heme b_3 iron and Fe_B, are present, was also established. On the basis of the structural analysis on the cyanide-bound enzyme, I will discuss the structural property of the substrate-bound form.

MATERIALS & METHODS

Purification of cNOR from P. aeruginosa

The cNOR used in this study was purified from anaerobically cultured *P. aeruginosa* (Kumita *et al.*, 2004). *P. aeruginosa* is grown at 30 ºC for 30 hours by 20 L of medium culture containing sodium glutamate monohydrate 10 g, KH_2PO_4 4.8 g, K_2HPO_4 6.0 g, KNO_3 5.0 g, $MgSO_4 \cdot 7H_2O$ 78.3 mg, $CuSO_4 \cdot 5H_2O$ 3.21 mg, $(NH_4)_6Mo_7O_{24} \cdot 4H_2O$ 0.45 mg, $FeCl_3 \cdot 6H_2O$ 3.0 mg, EDTA 6.0 mg, $CaCl_3 \cdot 2H_2O$ 1.5 mg / L. After this anaerobic static cultivation, *P. aeruginosa* is collected by centrifugation at 8,000 rpm for 10 min and stored at −80 ºC.

According to methods described elsewhere (Hino *et al.*, 2010; Kumita *et al.*, 2004), preparation of membranes was performed as below. The pellet of *P. aeruginosa* was suspended in 10 mM Tris-HCl buffer (pH 8.5) to reach the concentration of 10 g pellet/35 mL containing 1 mM EDTA and 1 mM phenylmethylsulfonylfluoride (PMSF). The mixture was sonicated at 4 ºC for 15 min and then centrifuged at 40,000 rpm for 1 h. The precipitation was suspended in 50 mM Tris-HCl (pH 8.5), 200 mM NaCl and then sonicated at 4 ºC for 15 min and then centrifuged at 40,000 rpm for 1 h. The precipitation was suspended in 20 mM Tris-HCl (pH 8.5) to the concentration of 27 mL/10 g-pellet and homogenated. The membrane fraction of *P. aeruginosa* was frozen and stored at −80 ºC until needed.

Purification of cNOR was performed by the reported method (Hino *et al.*, 2010; Kumita *et al.*, 2004) with minor modification. The membrane was thawed at room temperature and suspended in 20 mM Tris-HCl buffer (pH 8.5) to reach the concentration of 10 g pellet/35 mL. Triton X-100 (Sigma) was added to a final concentration of 2.5%. The mixture was gently stirred at 4 ºC for 2 h and then centrifuged at 125,000 x *g* for 1 h. The supernatant was put on top of 10-30% linear sucrose gradients in 10 mM Tris-HCl buffer (pH 8.5) containing 0.1% Triton X-100, and the gradients were centrifuged at 125,000 x *g* overnight at 4 ºC. The reddish brown band containing cNOR was collected manually and applied to 250-mL DEAE-sepharose column (GE Healthcare Bioscience), which was equilibrated with four column volumes of 20 mM Tris-HCl buffer (pH 8.5) containing 0.1% Triton X-100. The column was washed with two column volumes of equilibration buffer, and then the protein was eluted with a linear gradient of NaCl (0-0.3 M). The eluted fractions were collected and dialyzed against 20 mM Tris-HCl buffer (pH 8.5) containing 0.05% Triton X-100 overnight at 4 ºC. The proteins were subjected to second DEAE-sepharose column (volume: 80 mL) equilibrated with four column volumes of 20 mM Tris-HCl buffer (pH 8.5) containing 0.05% Triton X-100, and washed with 2 L of Tris buffer containing 0.05% DDM (Dojijdo) to exchange detergent. The bound proteins were eluted with Tris buffer containing 300 mM NaCl and 0.05% DDM, and then desalted using a HiPrep

26/10 desalting column (GE Healthcare Bioscience) with 50 mM potassium phosphate buffer (pH 7.5) containing 0.05% DDM. Fractions were applied to a CHT ceramic hydroxyapatite Type I column (Bio-Rad), which was pre-equilibrated with 50 mM potassium phosphate buffer (pH 7.5) containing 0.02% DDM. The column was washed with 1 L of equilibration buffer, and the enzyme was eluted with a potassium phosphate gradient (0.05-1 M). Fractions with A_{Soret}/A_{280} greater than 1.2 were concentrated by Amicon 30K (Millipore). An SP Sepharose HP column was employed as an additional, final step to control the homogeneity of phospholipid binding to cNOR. Some fractions were corrected by 0-20% of 20 mM HEPES buffer (pH 7.0), 1M NaCl, 0.02 % DDM, then each peak of cNOR, which has a A_{410}/A_{280} ratio greater than 1.5, was concentrated by Amicon Ultra-15 (Millipore). Purified cNOR was concentrated and rapidly frozen in liquid N_2 and stored at −80 ºC until needed.

The enzymatic activity of the purified cNOR was evaluated by using a Clark-type electrode equipped with an ISO-NO mark II system (World Precision Instruments) in a 0.9 mL anaerobic reaction chamber at 20 °C. The data were recorded on a Duo 18 (World Precision Instruments). The assay solution contained 50 mM Na citrate, pH 6.0, 0.1 % DTM, 10 mM glucose, 10 mg/mL catalase, 10 mg/mL glucose oxidase, and redox components. An aliquot of NO saturated buffer (50 mM Na citrate, pH 6.0) was added to the assay solution, and final concentration of NO was

approximately 10 mM. Once the background consumption of NO was stable, NO reduction (consumption) was initiated by the addition of cNOR (final concentration is 0.113 mM). The NO reduction rate of the purified cNOR was 433 ± 70 mM-NO/min/mM-NOR with ascorbate/phenazine methosulfate reduction system in 0.1 M sodium citrate pH 6.0, 0.1% (w/v) *n*-decyl-b-D-thiomaltoside (DTM) (Anatrace) at 20 °C, which is comparable to the values reported in the other NORs (Girsch & de Vries, 1997).

Crystallization of cNOR-Fab complex

The crystallization of cNOR with its antibody (Fab) is important to make high quality of cNOR crystals. Murine monoclonal antibody (clone #25) for co-crystallization of cNOR was generated and screened from ELISA positive clones. The Fab fragment from the antibody was prepared by proteolytic cleavage with papain and purified by anion exchange chromatography. The cNOR-Fab complex was formed by mixing the protein solutions at a stoichiometric molar ratio of 1:1.2 and excess Fab fragment was removed by gel filteration chromatography using buffer containing 0.1 % (w/v) of DTM (Anatrace). The eluted protein complex was concentrated with Amicon Ultra-4 (50K) to 20 mg/mL and used in co-crystallization experiments.

The micro-seeding method was applied to improve the quality of the cNOR crystals. The crystals used as seeds were obtained by former

experiments (Hino *et al.*, 2010). The crystals of 0.4 × 0.2 × 0.1 mm^3 were typically obtained by mixing 20 mg/ml cNOR-Fab complex dissolved in 20 mM HEPES buffer pH 7.0, 150 mM NaCl, 0.1% (w/v) DTM with an equal volume of the precipitant solution, micro seeds of cNOR crystal, 22-26% PEG400, 0.1 M sodium citrate pH 6.0, 10 mM $MgCl_2$, and 50 mM NaCl at 4 °C. Crystals appeared after one week and grew to full size within 2-3 weeks.

Preparation of cyanide-bound cNOR crystals

The cyanide-bound cNOR crystals were prepared by soaking methods. Prior to flash cooling, the crystals were soaked into cryoprotectant solution supplemented with 5 mM potassium cyanide by incrementally increasing the PEG400 concentration 2% at a time to 30%. The reduction procedure for the crystals was performed in cryo-protecting solution with 10 mM sodium dithionite at 4°C. After 90 min of soaking in the cryoprotectant solution containing dithionite, the color of the crystals changed from reddish brown to pink, indicating their reduction. To prepare the cyanide-bound reduced cNOR crystal, the reduced cNOR crystals were prepared in the presence of 5 mM potassium cyanide. The cyanide-bound reduced crystals were then flash-cooled in liquid nitrogen. The crystals of cyanide-bound cNOR were also prepared by alternative method. Before the crystallization, cyanide-bound cNOR was prepared by the addition of 5 mM cyanide to cNOR

in solution. Then, cyanide-bound cNOR was crystallized as the crystals of the oxidized form were prepared.

Data collection and structural refinement

X-ray diffraction data were collected on beamline 41XU at SPring-8 using radiation with a wavelength of 1 Å. The crystals were kept at 100 K during data collection. To reduce the radiation damage, the irradiated position was gradually moved during data collection. An image plate detector MX225HE CCD detector (Ryonix) was used to collect a 2.5 Å resolution data set. The data were processed using HKL2000 (Otwinowski & Minor, 1997). Data collection statistics are summarized in Table 1. Initial models were obtained by molecular replacement with Molrep (Vagin & Teplyakov, 1997) using the structure of the oxidized cNOR-Fab complex (PDB code: 3O0R) (Hino *et al.*, 2010) without water molecules or oxo ligand at the binuclear center as a search model. The structures were refined using Refmac5 (Vagin *et al.*, 2004) from CCP4 package. Water molecules were added to the atomic model at positive peaks greater than 2.5σ in the $F_o - F_c$ map and at position-appropriate hydrogen-bonding environments. For the active site, the Fe-C (cyanide) bond distance was restrained to 2.0 Å (refined to 2.01 Å), based on high resolution small molecular structures (WebCSD; http://webcsd.ccdc.cam.ac.uk/client_log_in.php?first_attempt=1). No angle restraints were used for the bound cyanide. More detailed refinement

procedures for the active site in ligand-bound cNOR are described in the Results and discussion section. Molecular visualization and model building were performed using COOT (Emsley & Cowtan, 2004). All structural figures were prepared using PyMOL (www.pymol.org).

Table 1. X-ray data and refinement statistics of cyanide-bound cNOR

	Cyanide-bound (oxidized)	Cyanide-bound (reduced)
Data collection		
Wavelength (Å)	1.0	1.0
Resolution (Å) [a]	35-2.5 (2.59-2.5)	35-2.5 (2.59-2.5)
Space group	$P2_12_12_1$	$P2_12_12_1$
Cell dimensions		
a (Å)	90.58	90.69
b (Å)	106.68	107.38
c (Å)	195.03	195.29
R_{merge} [a,b]	0.069(0.805)	0.075(0.529)
Completeness (%) [a]	99.4 (99.0)	99.1 (100.0)
Redundancy [a]	6.4 (5.6)	7.4 (7.4)
I/sigma (*I*) [a]	26.0 (2.3)	25.1 (3.8)
Refinement		
No. reflections	62090	62753
R_{work} / R_{free} [c]	0.177/0.224	0.189/0.227
No. atoms		
Protein	8061	8061
Ligand/ion	137	200
Water	243	242
Mean *B*-factors (Å^2)		
Protein	60.8	61.8
Ligand/ion	44.3	67.4
Water	57.1	53.2
R.m.s. deviation		
Bond length (Å)	0.020	0.015
Bond angles (°)	2.27	1.8
DPI (Å) [d]	0.202	0.205
Ramachandran plot [e]		
Favored region (%)	96.6	96.8
Outlier region (%)	0.3	0.4
PDB ID		3WFE

[a] Values in parentheses are for the highest-resolution shell.

[b] $R_{merge} = \Sigma_{hkl}\Sigma_i | I_i(hkl) - \langle I(hkl) \rangle | / \Sigma_{hkl}\Sigma_i I_i(hkl)$, where $\langle I(hkl) \rangle$ is the average intensity of *i* observations.

[c] $R_{work} = \Sigma_{hkl} | F_{obs}(hkl) - F_{calc}(hkl) | / \Sigma_{hkl} F_{obs}(hkl)$, where F_{obs} and F_{calc} are the observed and calculated structure factors, respectively. R_{free} was calculated with 5% of the reflections.

[d] Diffraction-data precision indicator (DPI) was calculated by Sfcheck (Vaguine *et al.*, 1999).

[e] Ramachandran plot analysis was obtained by Rampage (http://www.ncbi.nlm.nih.gov/pubmed/12557186) (Lovell *et al.*, 2003)

RESULTS & DISCUSSION

Improvement of purification and crystallization of cNOR

First crystal structure of cNOR from *P. aeruginosa* was reported with the resting oxidized state at a resolution of 2.7 Å (Hino *et al.*, 2010). Co-crystallization with cNOR antibody and using DTM as a detergent were critical to get crystals of high quality. However, the results of the crystallization and the resolution of the diffraction data often depend on the sample. Therefore I attempted to improve the purification method to constantly obtain high quality crystals. Since anion exchange column is used for the initial purification step, a action exchange chromatography of SP Sepharose HP column (GE) was performed as the additional and final step of purification to further purify *P. aeruginosa* cNOR. Unexpectedly, the eluted proteins from action exchange column were separated to six different peaks (Fig. 2). All six fractions exhibited only two bands assignable to the Nor and Norco subunits in SDS-PAGE and showed A_{Soret}/A_{280} = ~1.5, which is much better than that obtained before loading onto the action exchange column (A_{Soret}/A_{280} = ~1.3). In spite of these similar properties for each fraction, the ratio of cNOR/orthophosphate of each peak was different, suggesting that the amount of phospholipids (derived from the cellular membrane of *P. aeruginosa*) bound to cNOR was different in each peak. It was found that when each fraction of cNOR was separately used for crystallization, the

reproducibility in obtaining crystals remarkably increased. It can be concluded that the action exchange chromatography was important step for controlling the homogeneity of the phospholipids bound to cNOR and improving the change of crystal growth and the quality of the cNOR crystals.

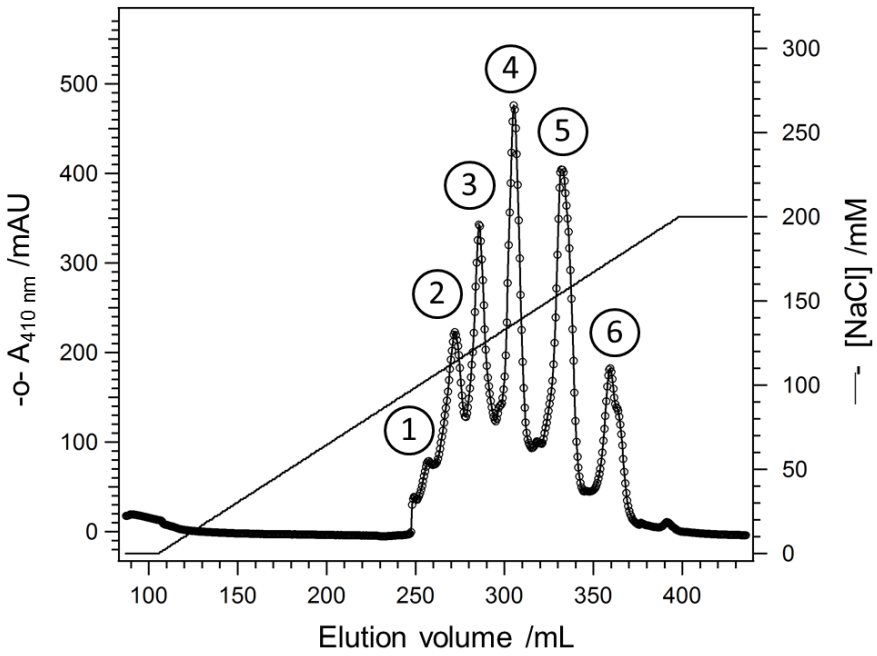

Figure 2. Elution profile obtained from a action exchange chromatography using SP sepharose HP column (GE). NOR fractions were separated to six peaks.

On the basis of preliminary diffraction experiments, I realized that larger crystals can diffract X-ray to higher resolution in this case of *P. aeruginosa* cNOR. The micro-seeding method was therefore applied to crystallize cNOR, because the micro seeds of the crystals generally accelerate the growth of the crystal core and eventually help crystal growth.

From the screening of wide variety conditions, I found that keeping the concentration of micro seeds in crystallizing solution low was crucial for obtaining high quality large crystals ($0.4 \times 0.2 \times 0.1$ mm^3). Combination of new purification method with micro seeding technique improved the quality of the cNOR crystals that give diffraction data with higher resolution at ~2.3 Å (vide infra).

Structure of Oxidized CN-bound cNOR

A previous study reported that cyanide binds at the active center of cNOR from *Paracoccus denitrificance* in the oxidized state and inhibits the NO reduction activity (Gronberg *et al.*, 2004). To confirm the cyanide binding to *P. aeruginosa* cNOR, the effect of cyanide on the NO reduction activity was examined at first. The addition of a ca. 60-fold molar excess of cyanide (40 mom KCN to 70 μM cNOR) completely inhibited the NO reduction activity of cNOR (data not shown). Next, we checked the binding of cyanide to the oxidized form of *P. aeruginosa* cNOR by monitoring the visible absorption spectrum and the inhibitory effect of cyanide. The addition of a ca. 1000-fold molar excess of cyanide (4 mom KCN to 4 μM cNOR) to the oxidized cNOR resulted in a red shift of the Soret band from 411 to 415 nm and an increase in the broad absorbance envelope of the low spin ferric hemes at 510-570 nm, while it took more than 10 hours to completely change the absorption spectrum (Fig. 3). Unusual slow kinetics for the cyanide

binding to oxidized cNOR (the rate constant was estimated to be 6.0 x 10^{-3} min^{-1}.), compared with the other heme-containing proteins like myoglobin, implies that the dissociation of the ox ligand bridging heme b_3 iron and Fe_B is required for the cyanide binding. These observations indicate that cyanide unambiguously binds to heme b_3 iron of *P. aeruginosa* cNOR in the oxidized state, as reported in *Pa. denitrificans* cNOR (Gronberg *et al.*, 2004).

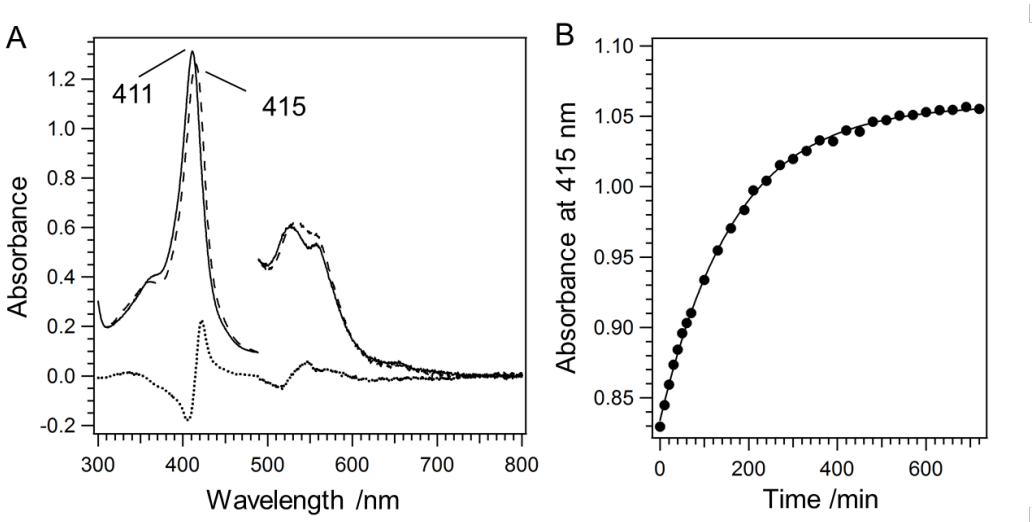

Figure 3. Changes of the absorption spectra of oxidized cNOR from *P. aeruginosa* upon addition of cyanide. (A) UV/vis absorption spectra of oxidized (solid curve) and cyanide-bound (broken curve) forms of cNOR. The difference spectrum (dotted curve) represents the effect of cyanide binding to oxidized form of cNOR. (B) Time course of the absorption change at 415 nm, absorption maximum of the cyanide-bound form, after the addition of cyanide to oxidized cNOR. Circles and solide curve represent the experimental data points and the single exponential fitting, respectively.

In order to prepare the crystals of cyanide-bound oxidized cNOR,

cyanide was added to oxidized cNOR prior to the crystallization set-up, and then the sample was crystallized. Using the purification and crystallization methods described above, an electron density map at a resolution of 2.5 Å was obtained. Very intense positive electron density with an oval sphere shape detected between heme b_3 and Fe_B in the unbiased $F_o - F_c$ map suggested the presence of cyanide at the active site (Fig. 4A). The Fe-Fe distance of 4.4 Å, which is longer than that of 3.8 Å in the resting state, provides further evidence of cyanide(s) binding to the binuclear center. Crystallographic refinements of the model with one cyanide bound to the heme iron resulted in significant residual density in $F_o - F_c$ map (Fig. 4B). Then, several possible models including two cyanide-bound structure or one cyanide with one oxygen atom were examined to fit to the density and refined by Refmac5 program to examine the resulting map and models. The most plausible model, obtained from comprehensive refinement, is shown in Figure 4. In this model, the occupancy of cyanides was estimated as 80%, and the remaining 20% was modeled as the oxo atom that derives from a resting state. The *B*-factors of these ligand atoms are in the range of 45-52 $Å^2$ which is similar to the *B*-factor of the heme iron (45-47 $Å^2$) and Fe_B (46-48 $Å^2$). Thus, the structure obtained from the crystals from cyanide-bound oxidized cNOR could be a mixture of multiple states such as cyanide-free and cyanide-bound oxidized forms. Since the dissociation of the oxo liand from the active site is seemed to be responsible for the cyanide binding,

cyanide-free form is still present in the crystals obtained from the oxidized enzyme with cyanide. An alternative possibility is that cyanide ion might be decomposed by hydrolysis reaction during the crystal growth, leading to less population of the cyanide-bound enzyme. It is also noteworthy that even the reduced form of cNOR may be present in the crystals due to the reduction of cNOR by hydrated electrons that are produced by the irradiation of strong X-ray to solvent water. Indeed, the electronic absorption spectrum of the cyanide-bound oxidized crystal used in the diffraction measurements showed an increase in absorption around visible region compared to that obtained before the irradiation of X-ray (data not shown), and indicated that some fractions of cNOR were reduced. It is therefore quite difficult to solve the structure of the cyanide-bound oxidized enzyme owing to the presence of different states in the crystal and at current resolution. On the basis of this finding, the reduced ligand-bound cNOR could be expected as a better target for precise structural analyses.

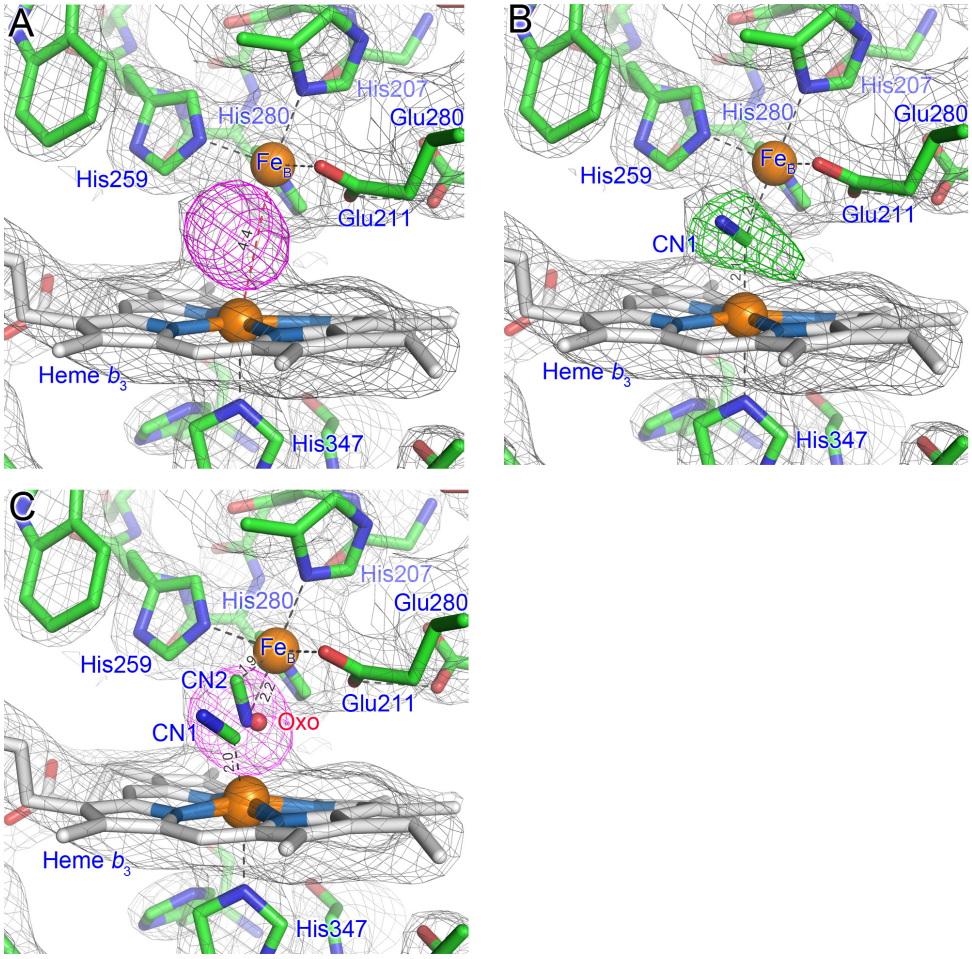

Figure 4. Electron density map of NO reduction site of the oxidized cyanide-bound form of *P. aeruginosa* cNOR. (A) F_o – F_c map at 8 σ (magenta) and $2F_o$-F_c map contoured at 1.4 σ (gray mesh) indicate the binding of cyanide(s). (B) F_o – F_c map at 4.0 σ (green mesh) after the crystallographic refinement in which one cyanide was tentatively modeled. Residual density in F_o – F_c map indicates the presence of additional atoms. (C) Proposed model for the oxidized cyanide-bound form of cNOR shows the binding of two cyanide molecules to the binuclear active center with 80% occupancy. The remaining 20% was modeled as the oxygen atom (oxo) that bridges two Fe atoms in a resting state. The unbiased omit map (magenta mesh) and 2 F_o – F_c map (gray mesh) are contoured at and 8.0 and 1.4 σ, respectively.

Structure of Reduced CN-bound cNOR

To test the cyanide binding to the reduced form of *P. aeruginosa* cNOR in the solution state, the UV/vis absorption spectra of the reduced state were measured both in the absence and the presence of cyanide (Fig. 5). The spectral changes were observed at the Soret and Q-band region by the addition of cyanide, while the spectral changes were less prominent than those reported for *Pa. denitrificans* cNOR (Gronberg *et al.*, 2004). Resonance Raman spectroscopy, which is sensitive to the coordination structure of heme, was utilized to confirm the cyanide binding to the reduced form of *P. aeruginosa* cNOR. In the reduced state, ν3, a coordination state marker for heme, was observed at 1493 and 1472 cm^{-1}, which are assignable to 6-coordinated ferrous heme and 5-coordinated ferrous heme, respectively. From the previous spectroscopic analysis on cNOR, we can suggest that the 5-coordinated species is derived from heme b_3. As seen in figure 6, loss of the ν3 mode at 1472 cm^{-1} upon the addition of cyanide indicates that cyanide binds to heme b_3 to form 6-coordinated ferrous heme. The cyanide binding to reduced cNOR was also supported by the disappearance of a heme iron-histidine stretching mode (νFe-His) at 217 cm^{-1} upon the addition of cyanide, since νFe-His is known to be only observed in 5-coordinated ferrous heme.

Crystals of the reduced CN-bound cNOR were prepared by soaking the crystals of the oxidized form into a solution containing reducing agent

(dithionite) and cyanide, and an electron density map at a resolution of 2.5 Å was obtained. The formation of the reduced CN-bound cNOR in the crystalline state could not be evaluated from the absorption spectrum because the binding of CN induced only a minor change in the Q-band and only intensified the Soret absorption in solution (Fig. 5), and a change in Soret absorption could not be precisely observed in the single-crystal absorption spectrum due to the saturation of the Soret absorption. However, the $F_o - F_c$ map showed intense electron density at the binuclear active center, which is indicative of the presence of cyanide ligand in the active site (Fig. 4). Slightly longer heme b_3 iron-Fe_B distance (4.4 Å) compared with that in the reduced state (4.2 Å) futher supports the binding of cyanide.

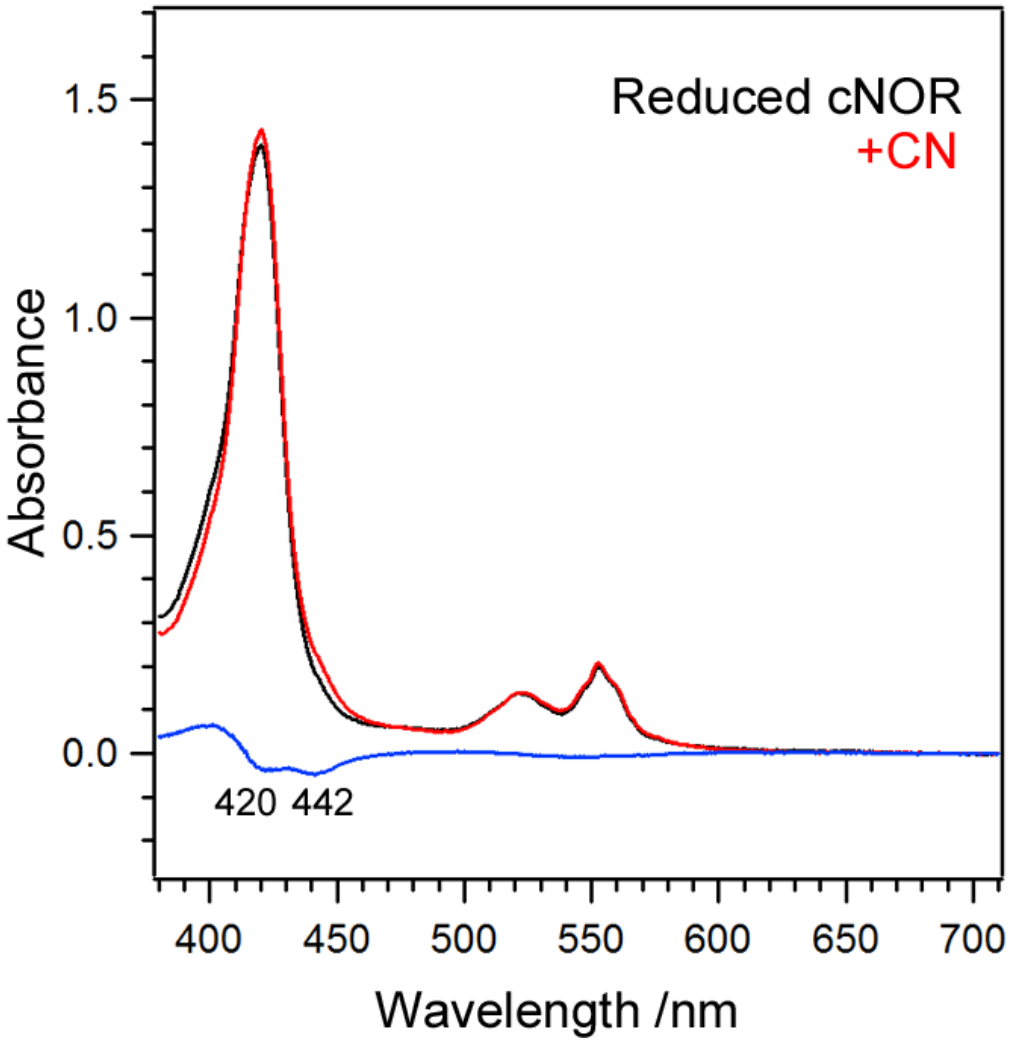

Figure 5. Optical absorption spectra for CN-bound cNOR. Panel shows optical absorption spectra for the solution state of reduced CN-bound cNOR. *Black* and *red* lines were obtained from reduced cNOR and reduced CN-bound cNOR, respectively. Blue lines indicate the difference between them. Spectra were obtained in 100 mM sodium citrate, pH 6.0, 50 mM NaCl, and 0.1% *n*-decyl-b-D-thiomaltoside.

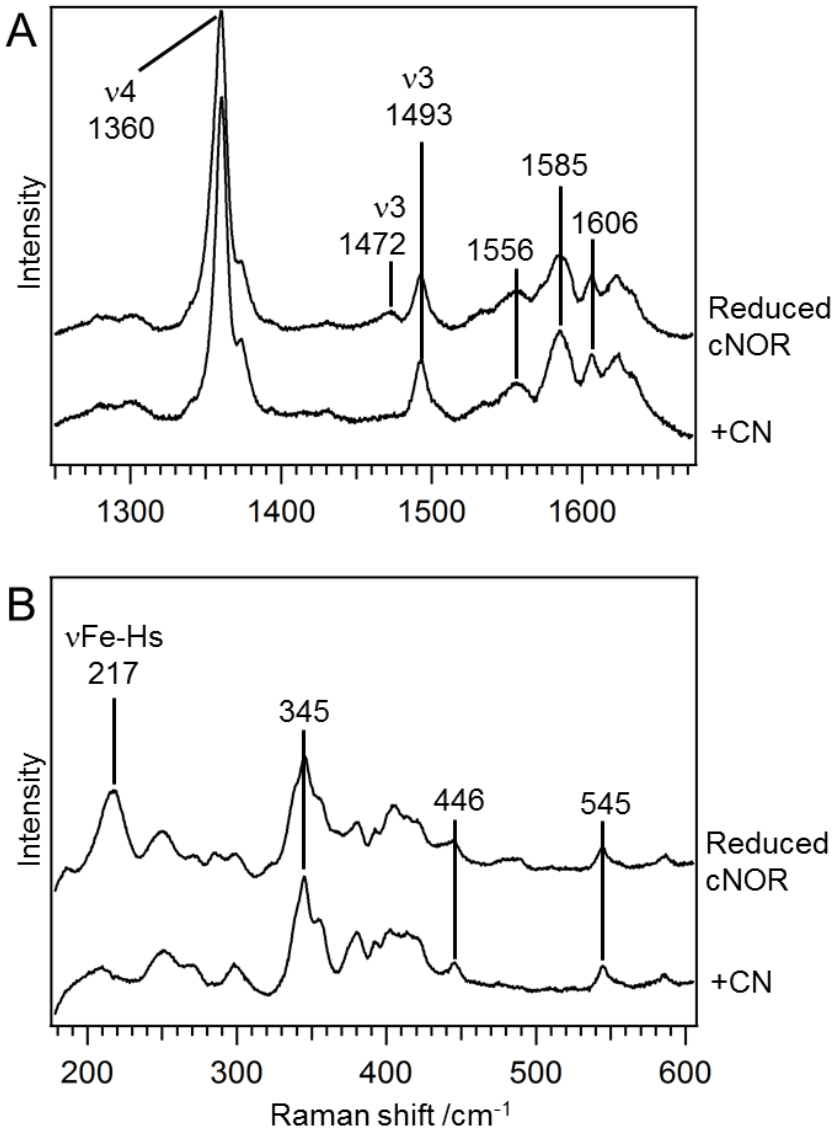

Figure 6. Resonance Raman spectra for reduced cNOR in the absence and presence of cyanide with 441.6 nm excitation. Panels (A) and (B) show high- and low-frequency regions of resonance Raman spectra, respectively. Traces shown were obtained from dithionite-reduced cNOR and reduced cNOR in the presence of 5 mM CN. The buffer used in the measurements was 100 mM sodium citrate, pH 6.0, 50 mM NaCl, and 0.1% *n*-decyl-b-D-thiomaltoside. The laser power was 1 mW at the sample point.

To determine the coordination structure of cyanide ion, I performed careful and comprehensive refinement at the active site of cNOR. An unbiased electron-density map ($F_o - F_c$) of the NO reduction site of the cyanide-bound reduced cNOR suggested more than two atoms existed at the active site. In other words, single cyanide binding cannot explain the electron density map. Furthermore, three atoms, e.g. single cyanide and one water molecule, are not sufficient for the $F_o - F_c$ map. These results and the previous studies on bovine CCO have suggested binding of two cyanide ions at the binuclear center (Fabian *et al.*, 2004), we, then, carried out crystallographic refinement with several types of two cyanides coordination structure.

In the best model, one of the cyanide ions coordinated to the heme b_3 with bent and tilted configuration toward the proposed substrates access channel (Fig. 7). Another cyanide ion was coordinated to the Fe_B in a side-on fashion (Fig. 7). The omit maps of each cyanide ion molecule also indicate that two cyanide ions are bound to the active center. The distance between the heme b_3 and the Fe_B was 4.4 Å, which is 0.6 Å longer than that of the oxidized cNOR, because of two cyanide ions coordinated to the narrow space of the active center. Cyanide molecules exhibit *B*-factor values (40-42 Å^2) similar to the average values for the other atoms in heme b_3 (40.9 Å^2), Fe_B (42.3 Å^2), heme ligand His347 (41.8 Å^2), and the three His ligands for Fe_B (44.6 Å^2), supporting the concomitant binding of two cyanide ions. An

improvement in the resolution, compared with those of the oxidized form, enabled us to identify a new water molecule that is involved in a hydrogen-bonding network, including conserved Glu215 near the active site (Fig. 8). It is also noteworthy that the coordination of amino acid ligands, His207, Glu211, His258 and His259, to Fe_B showed no change, even when two CN were bound to the binuclear active center.

Although the crystallographic refinement converged to the model with two cyanide ions bound structure without any repulsion between two cyanide ions, the distance between them is too close (~1.7 Å) as shown in Fig.7. The medium resolution (~2.5 Å) might not be sufficient to precisely build a model for small ligands in the active site of the CN-bound cNOR. The presence of two strong scatters, heme b_3 iron and Fe_B, creating a continuous density, also makes it difficult to interpret the density for multiple ligands. Indeed, the difficulty in determining the structure of the heme/Cu_B binuclear center at a medium resolution (2.25 Å) has also been reported for *P. denitrificans* CCO (Koepke *et al.*, 2009). While much higher resolution data is needed to determine more accurate structure of the reduced cyanide-bound cNOR, current data suggest that two cyanide ions can concomitantly bind to the active site of *P. aeruginosa* cNOR.

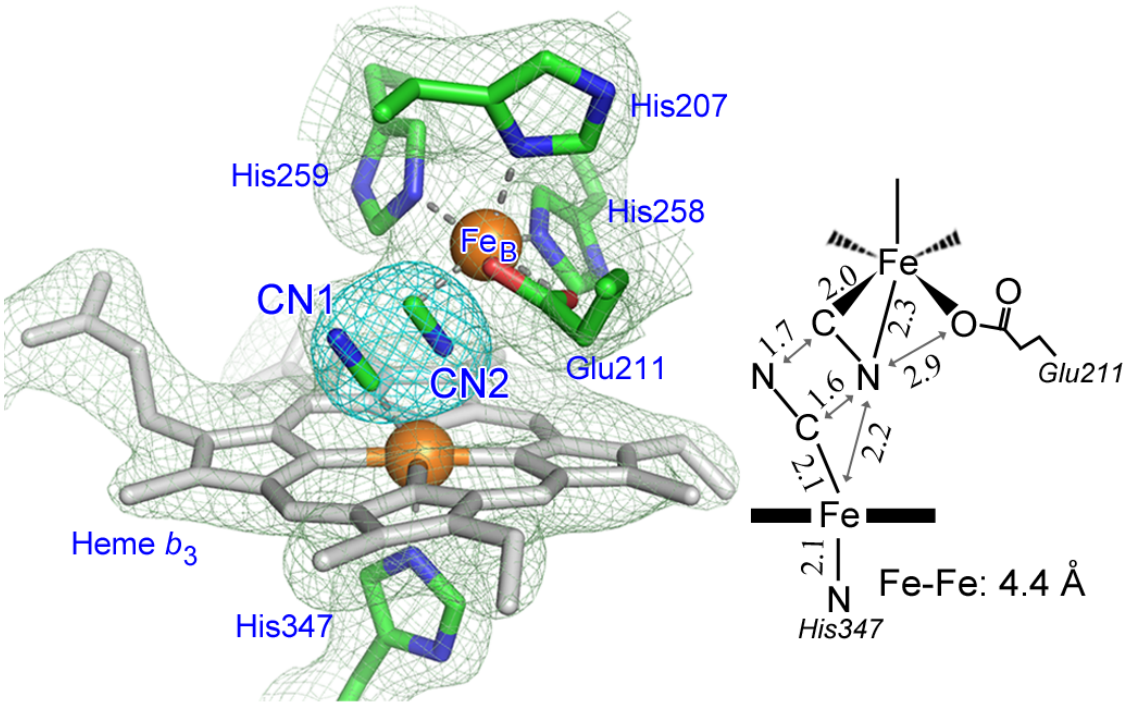

Figure 7. Structure of the NO reduction site of the reduced CN-bound form of *P. aeruginosa* cNOR. Light green mesh represents the 2*Fo-Fc* electron density map for the binuclear center at 1.5 σ for CN-bound cNOR. The *Fo-Fc* map (*cyn mesh*) countoured at 8 σ indicates the binding of CN. However, it was not possible to precisely determine the binding mode of CN. Structural characteristics at the binuclear active center are indicated as a schematic representation.

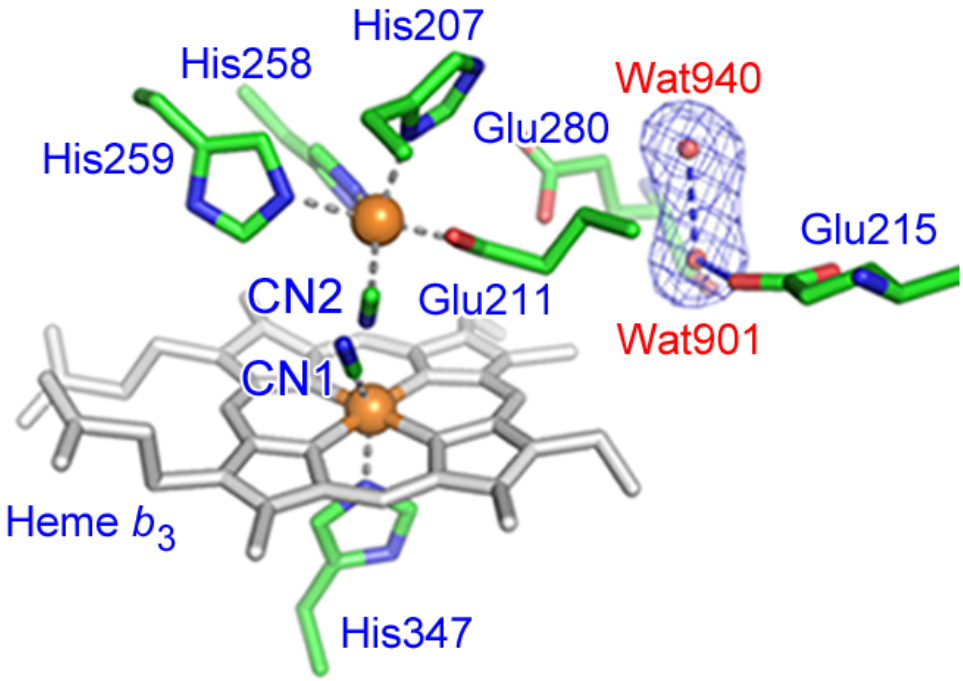

Figure 8. A newly observed water molecule in the reduced CN-bound forms of cNOR. Panel shows the omit maps at 5σ for the water molecules in CN-bound cNOR (2.5 Å resolution). Improvement of the data resolution in ligand-bound forms results in unambiguous density for two water molecules (Wat901 and Wat940) in the omit map.

Functional Implication from Structure of Cyanide-bound cNOR

The cyanide-bound form can be a good model for the substrate, NO, bound enzyme, because cyanide can bind to the active site both in oxidized and reduced states, like NO, and also strongly inhibits NO reduction activity. Thus, the structure of reduced cyanide-bound cNOR should provide insights into the structure of the substrate-bound form and catalytic mechanism of NO reduction by NOR. So far, three different mechanisms for the NOR-catalyzed reaction have been proposed (Moenne-Loccoz, 2007). In all proposed mechanisms, the binding of two NO molecules to the binuclear center is required for a formation of hyponitrite reaction intermediate via reductive N-N coupling. Current finding of the concomitant binding of two cyanide ions to the active site of cNOR is, therefore, functionally reasonable. The structure of reduced cyanide-bound form suggests that cNOR has an ability to concomitantly bind two diatomic molecules at the active site without large structural changes. I can propose from this observation that the active site of cNOR may be designed so as to keep two NO substrates in the confined space and to promote the formation of reductive N-N coupling.

Chapter 3

Structures of reduced and ligand-bound Nitric oxide reductase providing insights into functional differences in respiratory enzymes.

SUMMARY

Nitric oxide reductase (NOR) catalyzes the generation of nitrous oxide (N_2O) via the reductive coupling of two nitric oxide (NO) molecules at a heme/non-heme Fe center. We report herein on the structures of the reduced and ligand-bound forms of cytochrome *c*-dependent NOR (cNOR) from *Pseudomonas aeruginosa* at a resolution of 2.3-2.7 Å, to elucidate structure-function relationships in NOR, and compare them to those of cytochrome *c* oxidase (CCO) that is evolutionarily related to NOR. Comprehensive crystallographic refinement of the CO-bound form of cNOR suggested that a total of four atoms can be accommodated at the binuclear center. Consistent with this, binding of bulky acetaldoxime (CH_3-CH=N-OH) to the binuclear center of cNOR was confirmed by the structural analysis. Active site reduction and ligand binding in cNOR induced only a ~0.5 Å increase in the heme/non-heme Fe distance, but no significant structural change in the protein. The highly localized structural change is consistent

with the lack of proton-pumping in CCO. It also permits the rapid decomposition of cytotoxic NO in denitrification. In addition, the shorter heme/non-heme Fe length even in the bulky ligand-bound form of cNOR (~4.5 Å) than the heme/Cu distance in CCO (~5 Å) suggests the ability of NOR to maintain two NO molecules within a short distance in the confined space of the active site, thereby facilitating N-N coupling to produce a hyponitrite intermediate for the generation of N_2O.

INTRODUCTION

Nitric oxide reductase (NOR) is an integral membrane protein that is involved in microbial denitrification, a type of anaerobic respiration in which nitrate is reduced in a stepwise manner to dinitrogen ($NO_3^- \rightarrow NO_2^- \rightarrow NO \rightarrow N_2O \rightarrow N_2$). In this process, NOR catalyzes the reduction of nitric oxide (NO), which is generated as an intermediate product in this process, to nitrous oxide (N_2O) using two protons and two electrons ($2NO + 2H^+ + 2e^- \rightarrow N_2O + H_2O$) via N-N bond formation and N-O bond cleavage at a binuclear center consisting of heme and non-heme iron (Fe_B). The product of the NOR-catalyzed reaction, N_2O, is a greenhouse gas that is 310 times more powerful than carbon dioxide, and is also an ozone depleting substance (Ravishankara *et al.*, 2009). Since the use of nitrogen-based fertilizer increases global N_2O levels by stimulating the action of soil denitrifiers, NOR is an important topic of study in Earth science. NOR also has clinical and pharmaceutical importances, as evidenced by the fact that some pathogens use NOR to detoxify cytotoxic NO produced by macrophages in immune system of a host (Stevanin *et al.*, 2005).

In addition to being important in environmental and biological sciences, NOR is an attractive target for developing a better understanding of how the structures of respiratory enzymes are selected in nature in response to environmental changes. NOR shows sequence similarities to

cytochrome *c* oxidase (CCO), (e.g., the sequence identity is 10-16% between NOR and CCO (van der Oost *et al.*, 1994)), which is involved in the aerobic respiratory chain and pumps protons from the inside to the outside of the cell membrane in a process coupled with O_2 reduction ($O_2 + 4H^+ + 4e^- \rightarrow 2H_2O$) at a binuclear center consisting of heme and copper (Cu_B) (Saraste & Castresana, 1994; Zumft, 2005). Accordingly, NOR is classified as a member of the heme-copper oxidase superfamily, and is thought to originate from the same progenitor protein as CCO (Ducluzeau *et al.*, 2009; Pereira *et al.*, 2001; Saraste & Castresana, 1994; Sousa *et al.*, 2012). However, NOR and CCO exhibit distinct functional differences: NOR does not have any measurable proton-pumping activity (Hendriks *et al.*, 2002; Reimann *et al.*, 2007) and catalyzes the reduction of NO rather than O_2. Because NO was present in the atmosphere of the earth three billion years ago, but O_2 was not, one can imagine that this anaerobic respiratory enzyme, NOR, acquired proton-pumping ability when the catalytic activity changed from NO reduction to O_2 reduction during evolution of the respiratory enzymes. Thus, an understanding of the structure-function relationship in NOR and CCO would be highly desirable.

With respect to bovine and bacterial aa3 CCO (an A-type CCO) (Ferguson-Miller *et al.*, 2012; Lee *et al.*, 2012; Muramoto *et al.*, 2010; Pereira *et al.*, 2001; Qin *et al.*, 2009; Tsukihara *et al.*, 2003; Yoshikawa *et al.*, 1998) among CCOs; A-, B- and C-type CCOs (detailed definitions of the types of

CCOs have been reported elsewhere (Pereira *et al.*, 2001)), due to their available high-resolution crystal structures of oxidized, reduced and ligand-bound forms (e.g. CO-, NO-, and CN-bound forms), the mechanism behind the catalytic O_2 reduction and proton pumping activity has been extensively explored. A single molecular O_2 binds to the reduced heme iron, and the O-O bond is then cleaved by four electrons and four protons to give two water molecules via formation of ferryl reaction intermediate in the CCO (Ogura *et al.*, 1993). The structure of CCO indicated that conserved Tyr located at the active center, in addition to the redox active metal centers (heme a_3 iron and Cu_B), supplies electron to the O_2 ligand for catalytic four-electron reduction of O_2 (Muramoto *et al.*, 2010). Extensive structural analysis of CCO also revealed that the reduction of the redo centers and/or ligand binding to the active site induced structural changes in the proton transfer pathways and in the active site. Such structural changes are thought to be related to the gating function of the proton pumping activity coupled with catalytic O_2 reduction.

In contrast to CCO, structural information on NOR is limited. Earlier spectroscopic and theoretical studies on NOR provided insights into the function of NOR, and three possible mechanisms for the reduction of NO have been proposed (Blomberg & Siegbahn, 2012; Collman *et al.*, 2008; Kumita *et al.*, 2004; Moenne-Loccoz, 2007; Timoteo *et al.*, 2011). Using a rapid—freeze quenching technique, Kumara *et al.* reported on the

simultaneous observation of EPR signals arising from ferrous Fe_B-NO and ferrous heme-NO species during a single turnover reaction (Kumita *et al.*, 2004). They, therefore, suggested that a *trans* mechanism, in which one NO bound to heme b_3 reacts with another NO bound to Fe_B to produce a hyponitrite intermediate by reductive N-N coupling as the most plausible mechanism for the reduction of NO by NOR. However, their proposal based on the EPR results was criticized, i.e., our proposed reaction intermediate (ferrous heme b_3-NO/ferrous Fe_B-NO) would be EPR-silent most likely as the result of antiferromagetic coupling, and the EPR signals might arise from a mixture of ferrous heme b_3-NO/ferrous Fe_B and ferrous heme b_3/ferrous Fe_B-NO species (Moenne-Loccoz, 2007). In addition, theoretical calculations for the NOR-catalyzed reaction suggested that a *trans* mechanism is energetically unfavorable and *cis*-heme b_3 mechanism, in which a free NO molecule directly attacks a heme b_3 nitrosyl species, is the most likely explanation for the reaction (Blomberg & Siegbahn, 2012). The other mechanism, referred to as the *cis*-Fe_B mechanism, is characterized by the binding of two NO molecules at Fe_B to form a di-nitrosyl complex (Timoteo *et al.*, 2011). Despite the knowledge that has accumulated regarding the NOR reaction, the detailed mechanism for the NOR-catalyzed reaction remains unclear, mainly due to the paucity of structural information regarding NOR.

Hino *et al.* recently solved the crystal structures of two types of NORs in the resting state: cytochrome c-dependent NOR (cNOR) from

Pseudomonas aeruginosa and quinol-dependent NOR (qNOR) from *Geobacillus stearothermophilus* (Hino *et al.*, 2010; Matsumoto *et al.*, 2012). The active site Fe_B in NOR has a distorted original bipyramidal geometry, with three His ligands and one Glu ligand (Fig. 9), whereas the Cu_B in CCO adopts a distorted planar geometry, even though Cu_B also contains three His ligands in positions corresponding to the amino acid sequence of NOR. This difference in the coordination structure of non-heme metals could be due to the unique histamine-tyrosine cross-link that could permit CCO to shift the position of one of the His ligands for a non-heme metal. Essential Tyr that supplies electron to O_2 in CCO is absent in NORs, which is functionally reasonable, since the NO reduction by NOR requires only two electrons from heme b_3 iron and Fe_B, in contrast to four electrons required for O_2 reduction by CCO. Active site residues, therefore, could be a factor in the selection of the non-heme metal in the active site for NO or O_2 reduction. The reported structures of NORs provide some insights into the function; however, further structural studies are needed to elucidate the detailed mechanism for the NO reduction by NOR as well as the structural elements determining the function of the respiratory enzymes.

Given that the reduction and ligand-bound structures imply a mechanism that involves the catalytic O_2 reduction and coupled proton pumping in CCO (Ferguson-Miller *et al.*, 2012; Matsumoto *et al.*, 2012; Qin *et al.*, 2009; Tsukihara *et al.*, 2003; Yoshikawa *et al.*, 1998), the structures of

NOR in different states during the catalytic reaction, such as the reduced and ligand (substrate)-bound forms, would be invaluable in terms of elucidating the mechanism for the NOR reaction. In this study, in order to develop a better understanding of the structure-function relationships in NOR and the structural basis for the functional differences between CCO and NOR, we solved the crystal structures of *P. aeruginosa* cNOR in both the reduced state and reduced CO-bound state. Crystallographic refinement with various possible models provided information relative to the property of the active site of cNOR. I also found that the bulky acetaldoxime molecule (Ax: CH_3-CH=N-OH) binds to the active site of cNOR, and the structure of this form was also solved. On the basis of the structural information obtained from the current study and comparisons with CCO structures, the structural characteristics that govern NOR function are discussed.

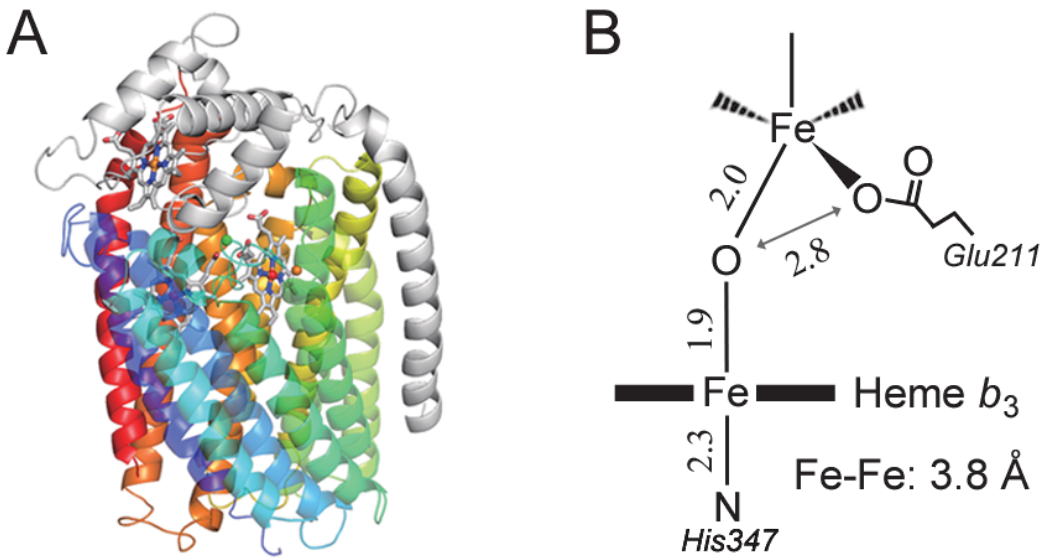

Figure 9. Structure of oxidized form of *P. aeruginosa* cNOR. (A) cNOR are composed of Nor B and Nor C subunits. The Nor B subunit is shown as colored ribbons; Nor C subunit, white ribbons. (B) The schematic representation of the active site in oxidized cNOR is shown for comparison.

MATERIALS & METHODS

Sample Preparation

The cNOR used in this study was purified from anaerobically cultured *P. aeruginosa*. The preparation of membranes and purification of cNOR were performed as described in previous studies (Hino *et al.*, 2010; Kumita *et al.*, 2004). An SP Sepharose HP column (GE) was utilized as an additional, and final step to control the homogeneity of the phospholipids bound to cNOR. The cNOR sample was loaded onto the column, which was equilibrated with 20 mom Hepes pH 7.0 and 0.02 % *n*-dodecyl-β-D-maltoside (Domino), and eluted with a linear gradient of 0-200 mom Nail. Each peak fraction of cNOR that had an A_{410}/A_{280} ratio greater than 1.5, was concentrated by means of an Amicon Ultra-15. The enzymatic activity of the purified cNOR was evaluated using a Clark-type electrode equipped with an ISO-NO mark II system (WPI). The NO reduction rate of the purified cNOR was 433±70 μM-NO/min/μM-NOR with an ascorbate/phenazine methosulfate reduction system in 0.1 M sodium citrate pH 6.0, 0.1 % (w/v) *n*-dodecyl-β-D-thiomaltoside (Anatrace) at 20 ℃, which is comparable to the values reported in the other NORs (Girsch & de Vries, 1997; Heiss *et al.*, 1989). The purified cNOR was stored at -80 ℃ until used. The Fab fragment from the antibody for the crystallization of cNOR was prepared by previously described methods (Hino *et al.*, 2010), and stored at -80 ℃.

Crystallization

The crystallization of the cNOR-Fab complex has been described previously (Hino *et al.*, 2010), and the micro-seeding method was applied to improve the quality of the cNOR crystals. Typically, 0.4 × 0.2 × 0.1 mm size crystals were obtained by mixing 20 mg/ml cNOR-Fab complex dissolved in 20 mom Hepes buffer pH 7.0, 150 mom Nail, 0.1 % (w/v) *n*-decyl-b-D-thiomaltoside with an equal volume of the precipitant solution, 22-26 % PEG400, 0.1 M sodium citrate pH 6.0, 10 mom $MgCl_2$, and 50 mom Nail at 4 °C. Prior to flash cooling, the crystals were soaked into a cryoprotectant solution supplemented with 10 mom sodium dithionite by incrementally increasing the PEG400 concentration 2% at a time to 30%. After 90 min of soaking in the cryoprotectant solution containing dithionite, the color of the crystals changed from a reddish brown to pink, indicating that reduction had occurred. The reduced crystals were then flash-cooled in liquid nitrogen. To prepare CO- or Ax- (CH_3-CH=N-OH) (Tokyo Chemical Industry) bound reduced cNOR crystals, the reduced cNOR crystals were prepared in the presence of either saturated CO, or 2 vole % Ax, respectively.

Data Collection and Refinement

X-ray diffraction data were collected on beamline 41XU at SPring-8 using an MX225HE CCD detector (Cryonics). The crystals were kept at 100

K during the data collection. To reduce the extent of radiation damage, the position of irradiation was gradually moved during the data collection. The data were processed using HKL2000 (Otwinowski & Minor, 1997). Data collection statistics are summarized in Table 2. Initial models were obtained by molecular replacement with Molrep (Vagin & Teplyakov, 1997) using the structure of the oxidized cNOR-Fab complex (PDB code: 3O0R) (Hino *et al.*, 2010) without water molecules or an ox ligand at the binuclear center as a search model. The structures were refined using Refmac5 (Vagin *et al.*, 2004) from the CCP4 package. Water molecules were added to the atomic model at positive peaks greater than 2.5 σ in the F_o – F_c map and at position-appropriate hydrogen-bonding environments. In the active site, the distance between irons and their coordinating atoms (from amino acid residues and exogenous ligands) was restrained during the refinement to 2.0-2.1 Å. More detailed refinement procedures for the ligand-bound cNOR are described in the Results section. Molecular visualization and model building were performed using COOT (Emsley & Cowtan, 2004). Table 2 summarizes the statistics for the data processing and refinement. All structural figures were prepared using PyMOL (www.pymol.org).

Spectroscopic Measurements

Optical absorption spectra of cNOR in the crystalline state were obtained at 100 K. The microspectrophotometer system consisted of a

deuterium tungsten halogen lamp (Ocean Optics, DT-MINI), Cassegrainian mirrors (Bunko-Keiki Co. Ltd.), an optical fiber, and a linear CCD-array spectrometer (Ocean Optics, SD2000) (Chiu *et al.*, 2006). Absorption spectra were corrected for the air blank baseline and dark reference. The crystalline sample for the spectroscopic measurement was prepared by the same method as that for the sample for the X-ray diffraction measurements. Optical absorption spectra in solution were recorded on a U-3010 spectrometer (Hitachi).

Resonance Raman spectra were obtained with a single polychromator (Join Yvonne, SPEX750M) equipped with a liquid nitrogen-cooled CCD detector (Roper Scientific, Spec 10:400B/LN). The 441.6 nm line from a He-Cod laser (Kinmon Electric, model CD4805R) was used for cNOR excitation. The laser power was adjusted to 1~5 mW at the sample point. Raman shifts were calibrated against indene and acetone. The measurements were performed with a spinning cell (~2,000 rpm) for sample concentrations of 20-40 mM.

Table 2. X-ray data and refinement statistics of reduced and ligand-bound cNOR

	Fully reduced	CO-bound (reduced)	Aldoxime-bound (reduced)
Data collection			
Wavelength (Å)	1.0	1.0	1.0
Resolution (Å) [a]	41-2.7 (2.80-2.70)	33-2.5 (2.59-2.50)	33-2.3 (2.38-2.30)
Space group	$P2_12_12_1$	$P2_12_12_1$	$P2_12_12_1$
Cell dimensions			
a (Å)	90.76	90.67	90.93
b (Å)	110.64	107.07	106.75
c (Å)	193.55	196.92	196.44
R_{merge} [a,b]	0.077 (0.823)	0.079 (0.555)	0.096 (0.783)
Wilson *B*-factor (Å^2)	63.67	47.39	49.60
Completeness (%) [a]	99.6 (99.5)	99.2 (100.0)	98.9 (100.0)
Redundancy [a]	4.0 (3.7)	3.8 (3.8)	7.0 (6.7)
I/sigma (*I*) [a]	16.0 (1.8)	15.5 (2.6)	16.3 (2.8)
Refinement			
No. reflections	51260	62441	78591
R_{work} / R_{free} [c]	0.202/0.250	0.191/0.232	0.191/0.232
No. atoms			
Protein	8061	8061	8061
Ligand/ion	131	200	200
Water	134	280	295
Mean *B*-factors (Å^2)			
Protein	80.8	55.1	60.7
Ligand/ion	69.9	54.6	64.2
Water	73.2	49.9	56.8
R.m.s. deviation			
Bond length (Å)	0.016	0.013	0.017
Bond angles (°)	1.7	1.8	1.9
DPI (Å) [d]	0.270	0.210	0.173
Ramachandran plot [e]			
Favored region (%)	96.5	96.4	97.2
Outlier region (%)	0.2	0.2	0.2
PDB ID	3WFB	3WFC	3WFD

[a] Values in parentheses are for the highest-resolution shell.

[b] $R_{merge} = \Sigma_{hkl}\Sigma_i | I_i(hkl) - \langle I(hkl)\rangle | / \Sigma_{hkl}\Sigma_i I_i(hkl)$, where $\langle I(hkl)\rangle$ is the average intensity of *i* observations.

[c] $R_{work} = \Sigma_{hkl} | F_{obs}(hkl) - F_{calc}(hkl) | / \Sigma_{hkl} F_{obs}(hkl)$, where F_{obs} and F_{calc} are the observed and calculated structure factors, respectively. R_{free} was calculated with 5% of the reflections.

[d] Diffraction-data precision indicator (DPI) was calculated by Sfcheck (Vaguine *et al.*, 1999).

[e] Ramachandran plot analysis was obtained by Rampage (http://www.ncbi.nlm.nih.gov/pubmed/12557186) (Lovell *et al.*, 2003).

RESULTS

Structure of Reduced cNOR

To prepare crystals of the reduced form of *P. aeruginosa* cNOR, we reduced ferric cNOR crystals by soaking them in a dithionite solution. Complete reduction of the cNOR crystal was confirmed by the single-crystal absorption spectrum, in which peaks were observed at 522 and 553 nm (Fig. 10); these peaks are characteristic of the reduced form of cNOR in solution. The single-crystal spectra were identical before and after the diffraction measurements (Fig. 10), indicating that the oxidation states of heme and non-heme iron in the fully reduced form were not altered as the result of the X-ray irradiation. The structure of dithionite-reduced cNOR solved at a resolution of 2.7 Å was nearly identical to that of the oxidized form, except at the binuclear center.

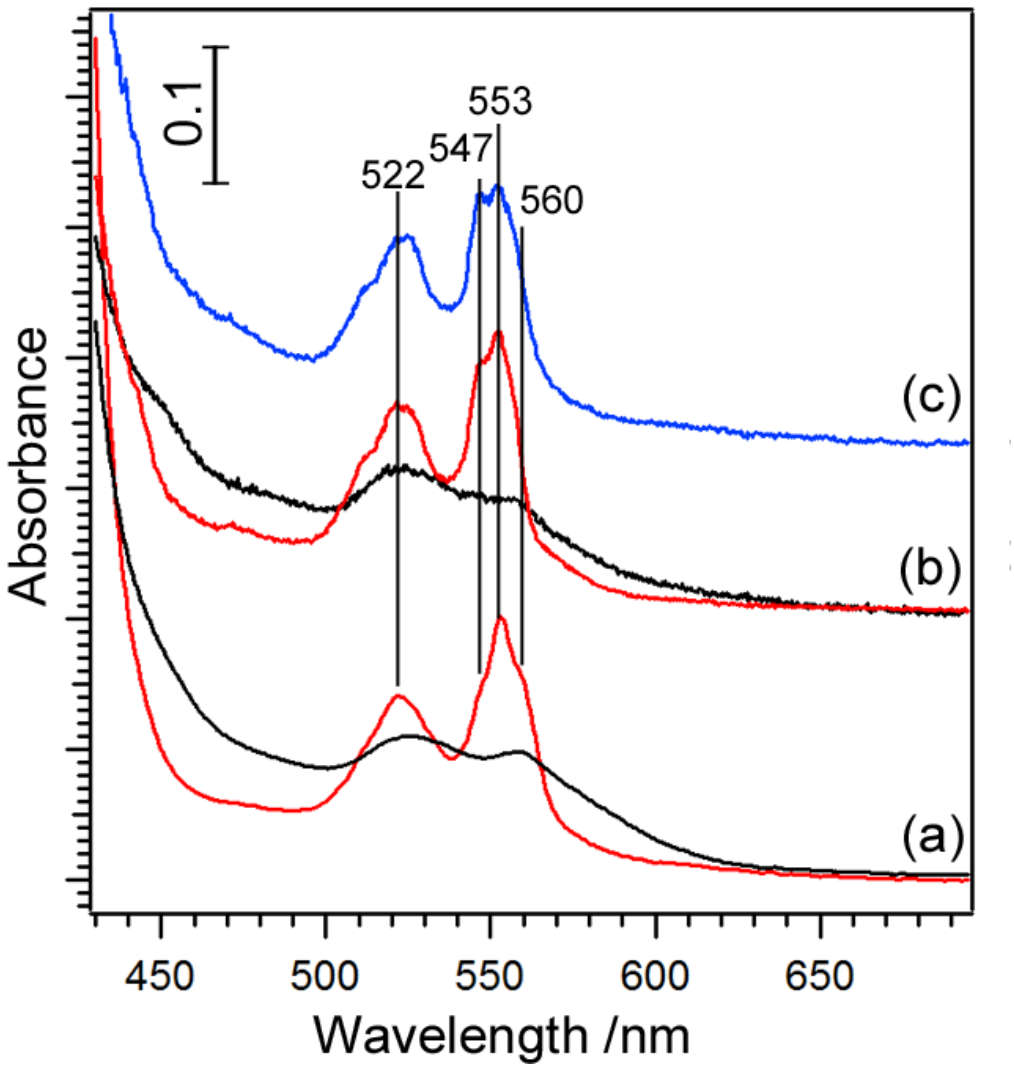

Figure 10. Optical absorption spectra for cNOR. Panel shows the spectra for the solution (a) and crystalline (b) states. *Black* and *red* lines were obtained from oxidized and dithionite-reduced cNOR, respectively. Blue line was obtained from dithionite-reduced cNOR after the diffraction measurement (X-ray irradiation for 30 min).

At the binuclear center of the reduced cNOR, the intense positive peak near Fe_B in the $F_o - F_c$ map suggests that, instead of the bridging ox ligand present in the oxidized cNOR (Fig. 9), a ligand is bound to Fe_B (Fig. 11). Refinement with a water molecule or a hydroxide ion gave a residual positive peak in the $F_o - F_c$ map, which indicates that a more electron-rich ligand would be bound to Fe_B. Since the crystallization solution contains Nail and $MgCl_2$, we carried out a refinement with chloride (Cal^-) to determine the nature of the ligand for Fe_B in the reduced cNOR, and found that there was no residual peak greater than 3 σ in the $F_o - F_c$ map. A distance of 2.5 Å between Cal^- and Fe_B is also consistent with the binding of Cal^- to Fe_B, but not bound to heme b_3 (heme b_3 Fe-Cal^- distance: 2.8 Å) (Fig. 11). The distance of His347-heme b_3 iron was 2.0 Å, indicating that heme b_3 is a 5-cooridinate structure. The absence of the heme b_3 ligand (bridging ox ligand) is consistent with the resonance Raman data in solution, which showed that heme b_3 iron adopted a 5-coordinate state in its reduced form, because the n_3 mode, a heme oxidation state marker, at 1472 cm^{-1} is derived from 5-coordinate ferrous heme (Fig. 12). In addition, the Raman line at 217 cm^{-1} was observed only in the ferrous heme with 441.6 nm excitation (Fig. 12), and was not observed in the 6-coordinate ferrous heme such as in the CO-bound form. I therefore assigned this 217 cm^{-1} band to the heme Fe-His317 stretching mode of the 5-coordinate ferrous heme (Kitagawa, 1988). A similar structure has also been proposed for reduced cNOR from

Paracoccus denitrificans in solution (Moenne-Loccoz & de Vries, 1998). With the absence of the bridging ox ligand, the Fe-Fe distance was longer in the reduced cNOR (4.2 Å) than in the oxidized cNOR (3.8 Å). In spite of the increased Fe-Fe distance, the coordination of amino acid ligands including Glu211 to Fe_B was retained by the reduction of the active site.

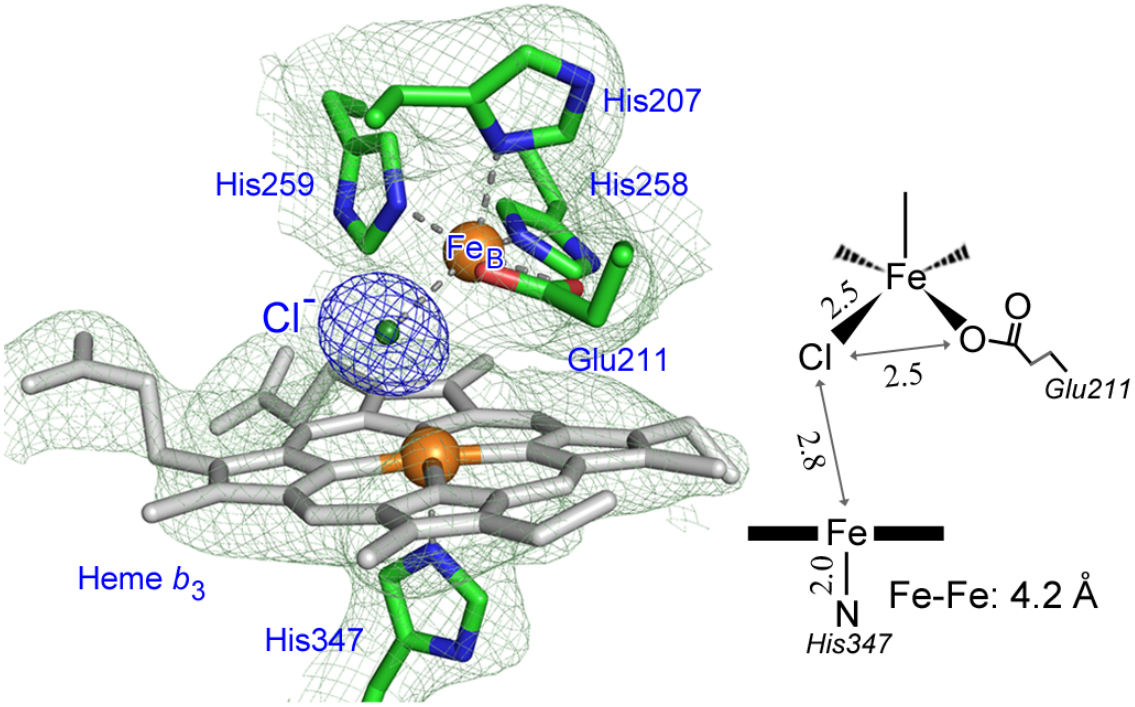

Figure 11. Structure of the NO reduction site of the reduced form of *P. aeruginosa* cNOR. Light green mesh represents the 2*Fo-Fc* electron density map for the binuclear center at 1 σ for reduced cNOR. The *Ft-C* map (*blue mesh*) countoured at 10 σ indicates the binding of Cal^-. Structural characteristics at the binuclear active center are indicated as a schematic representation.

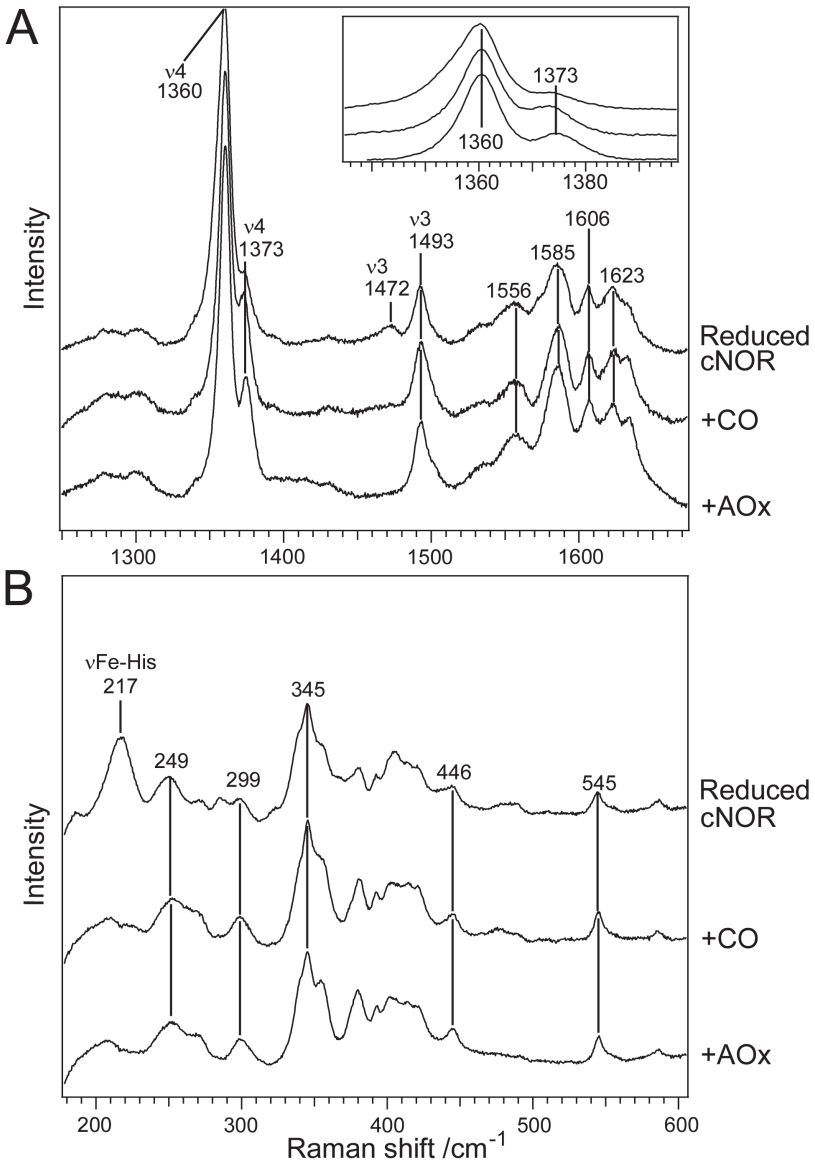

Figure 12. Resonance Raman spectra for cNOR with 441.6 nm excitation. Panels (A) and (B) show high- and low-frequency regions of resonance Raman spectra, respectively. Inset in panel (A) shows the enlarged n4 region of the spectra. Traces shown were obtained from dithionite-reduced cNOR, reduced cNOR in the presence of saturated CO, or 0.1 vole % acetaldoxime (Ax). The buffer used in the measurements was 100 mom sodium citrate, pH 6.0, 50 mM Nail, and 0.1% *n*-decyl-b-D-thiomaltoside. The laser power was 1 mW at the sample point.

Structure of Reduced CO-bound cNOR

Crystals of the reduced CO-bound cNOR were prepared by the soaking method, and an electron density map at a resolution of 2.5 Å was obtained. The formation of the CO-bound cNOR could not be evaluated from the absorption spectrum because the binding of CO induced only a minor change in the Q-band and only intensified the Soret absorption in solution (Fig. 13), and a change in Soret absorption could not be precisely observed in the single-crystal absorption spectrum due to the saturation of the Soret absorption. However, an unbiased $F_o - F_c$ electron density map of the active site of the reduced CO-bound cNOR showed a rhomboidal shape between the two iron atoms, indicating the presence of CO molecule(s) at the binuclear center (Fig. 14). The Fe-Fe distance increased to 4.4 Å mainly due to the shift of the Fe_B atom by 0.3 Å from its position in the reduced cNOR, providing further evidence of CO binding to the binuclear center. Comparing the structure of the reduced CO-bound form with that of the oxidized or reduced form, no substantial structural changes were evident in the overall structure, but structural differences were observed at the binuclear center. An improvement in the resolution, compared with those of the oxidized and reduced forms, enabled us to identify a new water molecule that is involved in a hydrogen-bonding network, including conserved Glu215 near the active site (Fig. 15). It is also noteworthy that the coordination of amino acid ligands, His207, Glu211, His258 and His259, to Fe_B showed no change, even

when the CO was bound to the binuclear active center.

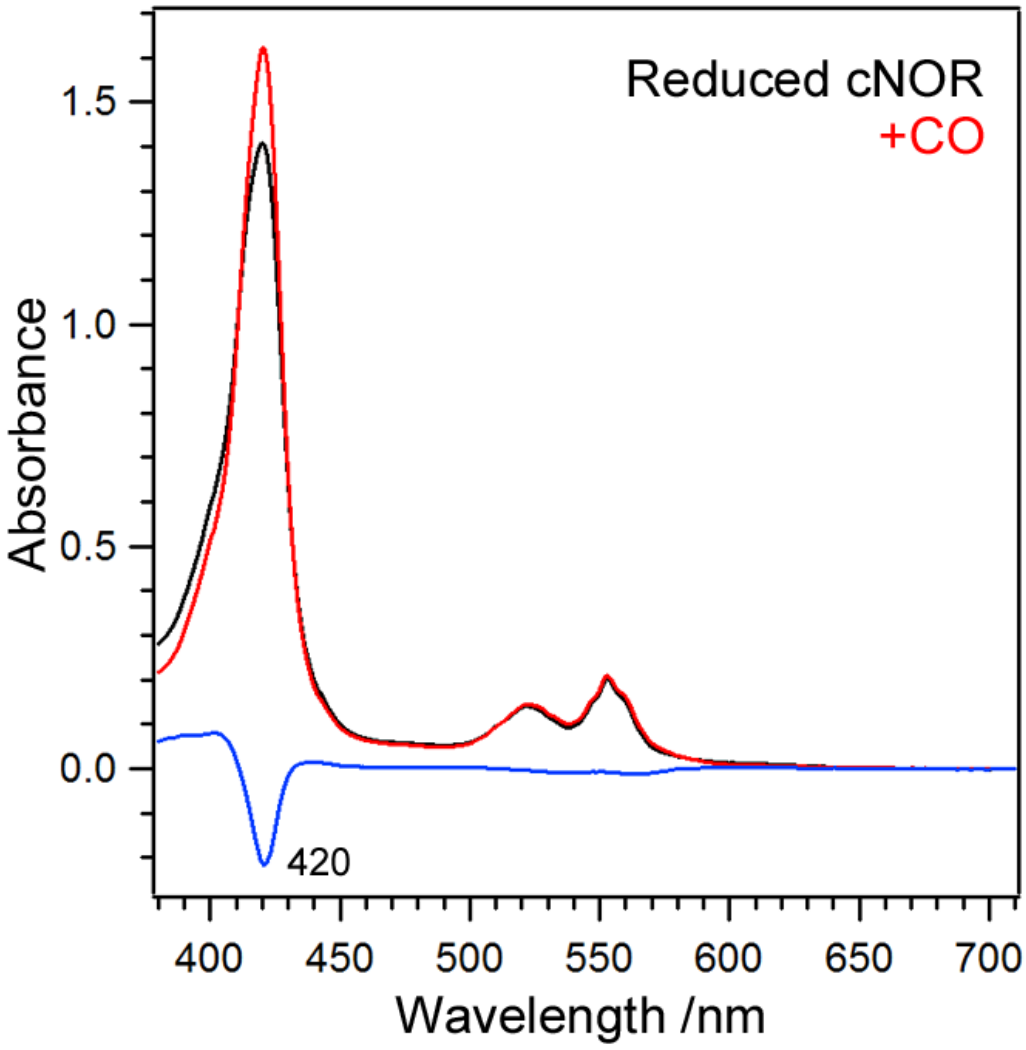

Figure 13. Optical absorption spectra for CO-bound cNOR. Panel shows optical absorption spectra for the solution state of reduced CO-bound cNOR. Black and red lines were obtained from reduced cNOR and reduced CO-bound cNOR, respectively. Blue lines indicate the difference between them. Spectra were obtained in 100 mM sodium citrate, pH 6.0, 50 mM Nail, and 0.1% *n*-decyl-b-D-thiomaltoside.

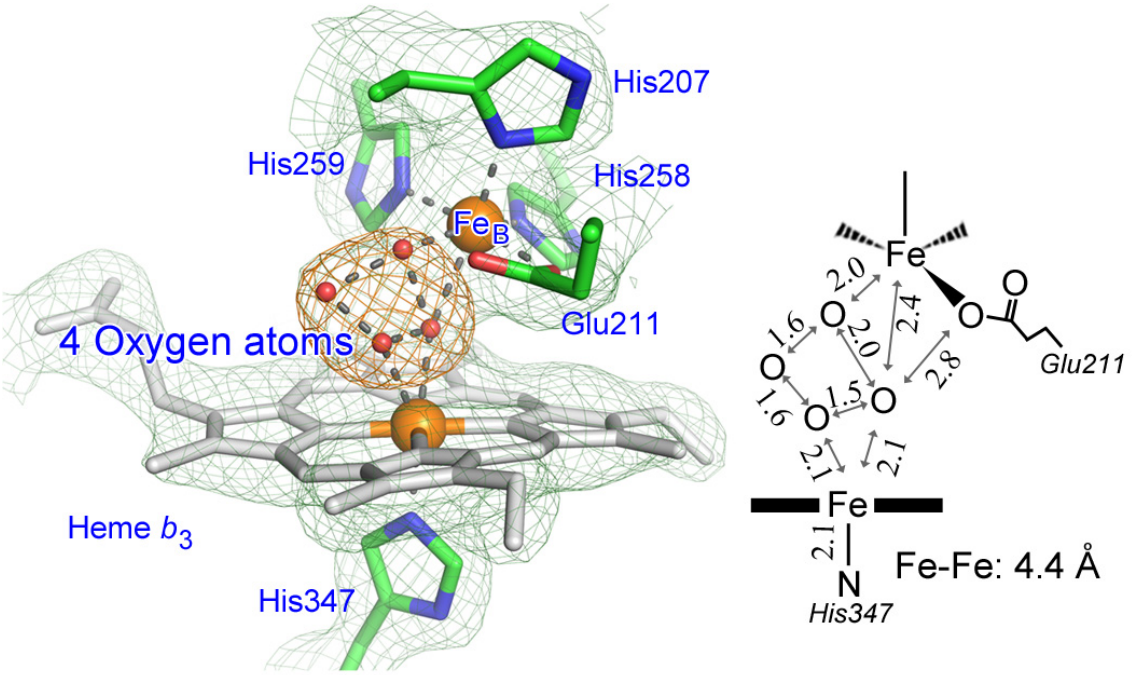

Figure 14. Structure of the NO reduction site of the reduced CO-bound form of *P. aeruginosa* cNOR. Light green mesh represents the 2*Fo-Fc* electron density map for the binuclear center at 1.5 σ for CO-bound cNOR. The *Ft-C* map (*orange mesh*) countoured at 8 σ indicates the binding of CO. However, it was not possible to precisely determine the binding mode of CO. The model structure shown was obtained by a refinement without any distance restrains for four oxygen atoms. Structural characteristics at the binuclear active center are indicated as a schematic representation.

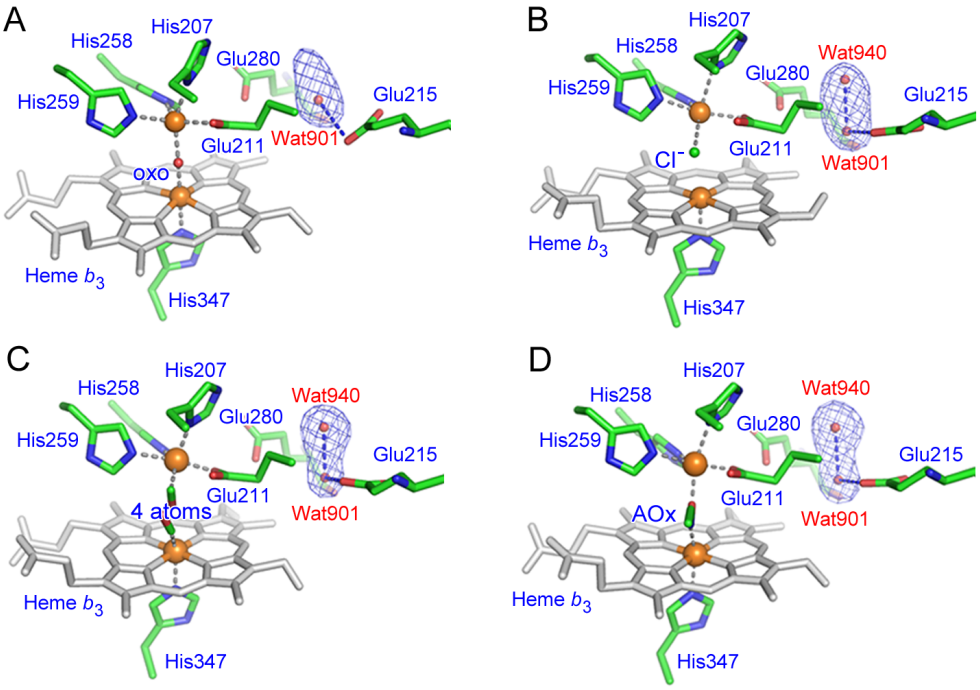

Figure 15. Newly observed water molecules in the reduced ligand-bound forms of cNOR. Panel (A) shows the omit map near conserved Glu contoured at 4σ calculated from data of oxidized cNOR at 2.7 Å resolution. One water molecule (Wat901) was modeled in our previous study (PDB code 3O0R). Panel (B) shows the omit map at 3σ calculated from data for the reduced form of cNOR at 2.7 Å resolution. Panels (C) and (D) show the omit maps at 5σ for the water molecules in CO-bound (2.5 Å resolution) and Ax-bound forms (2.3 Å resolution) of cNOR, respectively. Improvement of the data resolution in ligand-bound forms results in unambiguous density for two water molecules (Wat901 and Wat940) in the omit map. These data suggest that the oxidized or reduced cNOR also have two water molecules in the ellipsoidal density.

In order to determine the structure of the active site, we first performed a crystallographic refinement with a single CO molecule. However, the refinement resulted in a very low *B*-factor for the CO ligand and still gave a distinct positive peak in the $F_o - F_c$ map at the binuclear center (Fig. 16A), indicating that the presence of only a single CO molecule at the active site failed to explain the electron density observed between heme b_3 and Fe_B. I then carried out a refinement by constructing several possible models for the CO-bound structure, to determine the binding mode of the CO molecule. Since Cal^- coordinates to Fe_B in the reduced cNOR structure, models containing one CO molecule and one Cal^- (or water) were examined. However, the models failed to fit the electron density map, which was evident from the resulting $F_o - F_c$ map after the refinement (Fig. 16B). I also tested the possibility of multiple conformations of a single CO molecule at the binuclear center, that is, a mixture of the different CO-bound structures: one is a heme b_3-CO species and the other a Fe_B-CO species. When the occupancies of the two CO molecules were fixed at 50% each in the model refinement, the resulting $F_o - F_c$ map showed a highly positive density (5σ) over the space between heme iron and Fe_B, which would exclude multiple conformations of CO. All of the models discussed above are unlikely.

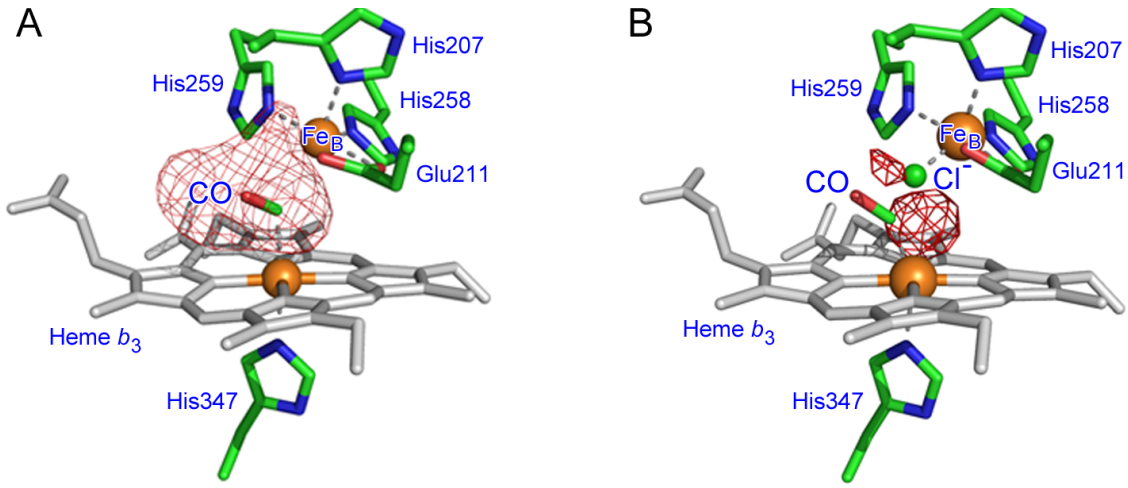

Figure 16. Detailed refinements for the reduced CO-bound form of cNOR. Panel (A) shows the $F_o - F_c$ map (*red mesh*) obtained by the refinement with single CO molecule at the binuclear center. The $F_o - F_c$ map is contoured at the 3s level. Strong electron density in $F_o - F_c$ map indicates that the single CO molecule cannot explain the electron density observed at the binuclear center. Panel (B) shows the $F_o - F_c$ map (*red mesh*) obtained by the refinement with single CO molecule and Cal^- at the binuclear center. The $F_o - F_c$ map is contoured at the 3 σ level. Extra electron density was still observed, indicating that the combination of single CO molecule and Cal^- also cannot explain the electron density observed at the binuclear center.

Refinement without any distance restraint for four oxygen atoms was performed. The refinement converged to the model with all oxygen atoms still accommodated within the density of the $2F_o - F_c$ map. No residual electron density greater than 3σ in the $F_o - F_c$ map appeared (Fig. 14). Furthermore, the *B*-factor values for four oxygen atoms (36.6, 44.6, 45.8 and 34.2 Å^2) are comparable to the average values for heme b_3 (41.3 Å^2), the nitrogen atoms of three histamine ligands for Fe_B (43.8 Å^2), and Fe_B (43.2 Å^2), which is indicative of the presence of four atoms each with 100% occupancy at the binuclear center in cNOR. These observations raise the possibility that, at most, a total of four atoms; e.g. two CO molecules or one CO molecule plus two water molecules, could be accommodated in the binuclear active center in cNOR. Various combinations of coordination and orientation of two CO molecules were then fit to the rhomboidal electron density and refined using the Refmac5 program with a 100% occupancy of CO and distance restrains of 2.0 Å for the heme b_3 Fe-CO and Fe_B-CO bonds and 1.23 Å for C-O bond. The refinement gave two possible models with the concomitant binding of two CO molecules to the binuclear active center (Figs. 17).

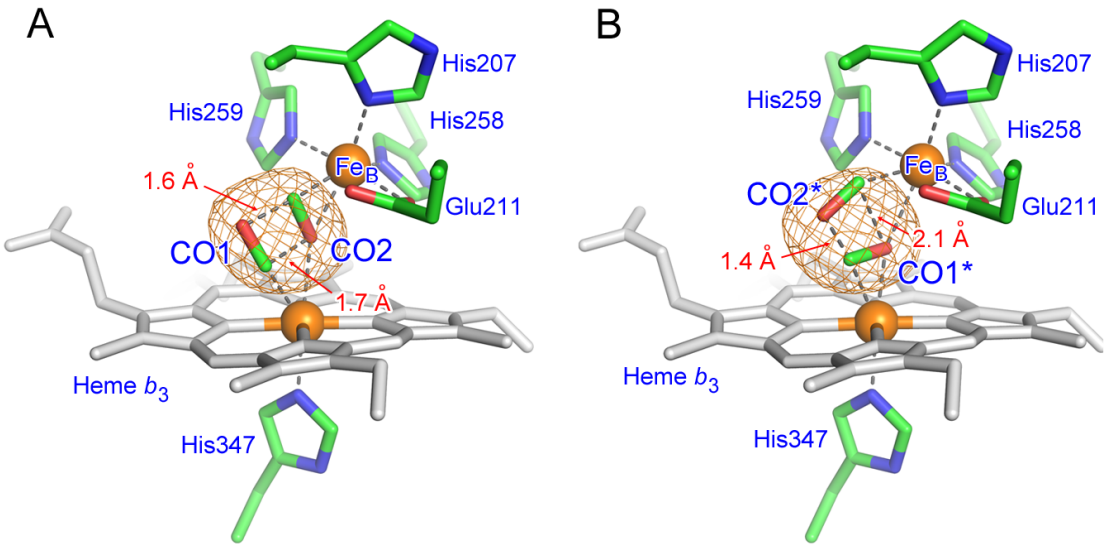

Figure 17. Proposed models for the reduced CO-bound form of cNOR. Panels (A) and (B) show two possible models with the simultaneous binding of two CO molecules to the binuclear active center. *Orange mesh* shows the $F_o - F_c$ map (8 σ) obtained by omitting the CO ligands. This model satisfies with the crystallographic data. However, the distance between two CO molecules is too close.

The $F_o - F_c$ maps calculated from both of the final models, with an occupancy of 100% for the two CO molecules, showed no significant residual density in the active site, indicating that concomitant binding of two CO molecules explained the electron density. In addition, the *B*-factor values around the active site were reasonable; the atoms of the two CO molecules exhibit *B*-factor values (40-42 Å^2) similar to the average values for the other atoms in heme b_3 (40.9 Å^2), Fe_B (42.3 Å^2), heme ligand His347 (41.8 Å^2), and the three His ligands for Fe_B (44.6 Å^2). However, two CO molecules, which were refined to a distance of 1.4 or 1.6 Å, are too close to belong to different molecules. Similarly, the refinement of a model, in which one CO molecule and two water molecules are located at the active site, also converged without ligand repulsion, although the distances between the CO and water molecules were very close (~1.5 Å) (Fig. 18). The medium resolution (~2.5 Å) might not be sufficient to precisely build a model for small ligands in the active site of the CO-bound cNOR, in which the presence of two strong scatters, heme b_3 iron and Fe_B, creating a continuous density, also makes it difficult to interpret the density for multiple ligands. Indeed, the difficulty in determining the structure of the heme/Cu_B binuclear center at a medium resolution (2.25 Å) has also been reported for *P. denitrificans* CCO (Koepke *et al.*, 2009). The results of our crystallographic refinement of many possible models for the CO-bound cNOR indicate a total of four atoms are present at the active site in cNOR.

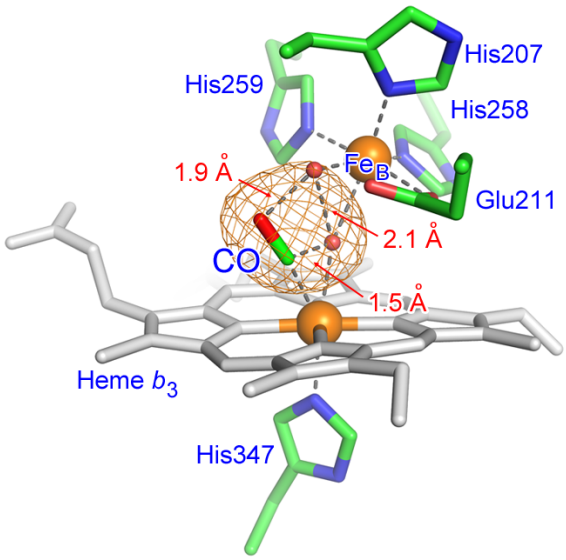

Figure 18. Alternative model for the reduced CO-bound form of cNOR. Panel shows the model structure refined with single CO and two water molecules. This model could also explain the electron density map, although the distances between CO and water molecules are very close.

Structure of Reduced Aldoxime-bound cNOR

The finding that the active site potentially accommodates four atoms; e.g. two CO molecules, in the reduced CO-bound cNOR would be related to the functional properties of cNOR, because two diatomic substrates, NO (total of four atoms), are required to bind at the active site, and a hyponitrite, $N_2O_2^{2-}$ (a four atomic molecule), bound form is suggested as a possible reaction intermediate in ANY proposed reaction mechanism in NOR (Moenne-Loccoz, 2007). It would be very interesting to examine and characterize the binding of four atomic or larger molecules to the binuclear active center of cNOR for a better understanding of the structure-function relationship in NOR.

I explored possible bulky ligands for the binuclear active center by monitoring the UV/visible absorption spectrum which is sensitive to ligand binding. We found that the addition of Ax (CH_3-CH=N-OH) to the reduced cNOR increased the absorbance of the Soret band (Fig. 19). Given that Ax can bind to the heme iron in aldoxime dehydratase (Ox) during catalysis (Sawai *et al.*, 2009), our observation implies that Ax could function as a ligand for heme b_3 in cNOR. The binding of Ax to heme b_3 iron was confirmed by a change in the resonance Raman spectrum upon adding Ax to the reduced cNOR. As shown in Figure 12, the n3 and the Fe-His stretching modes arising from ferrous 5-coordinate heme b_3 disappeared upon the addition of Ax to the reduced cNOR, indicating the successful binding of Ax

to heme b_3. It is also noteworthy that the binding of Ax to heme b_3 resulted in the appearance of the n4 mode at 1373 cm^{-1} (Fig. 12). A similar spectral change in the n4 mode was induced by the binding of CO to ferrous heme (Fig. 12), which was interpreted as an increase in the ferric character of the heme iron due to π backdonation from the Fe *d* orbital to the CO *p* orbital. Since the n4 mode is shifted to a higher frequency in butyraldoxime-bound Ox (Oinuma *et al.*, 2005), and the nitrogen atom of aldoxime binds to ferrous heme in Ox (Sawai *et al.*, 2009), this suggests that the nitrogen atom of Ax coordinates to the heme b_3 iron in the reduced cNOR, as was observed in Ox.

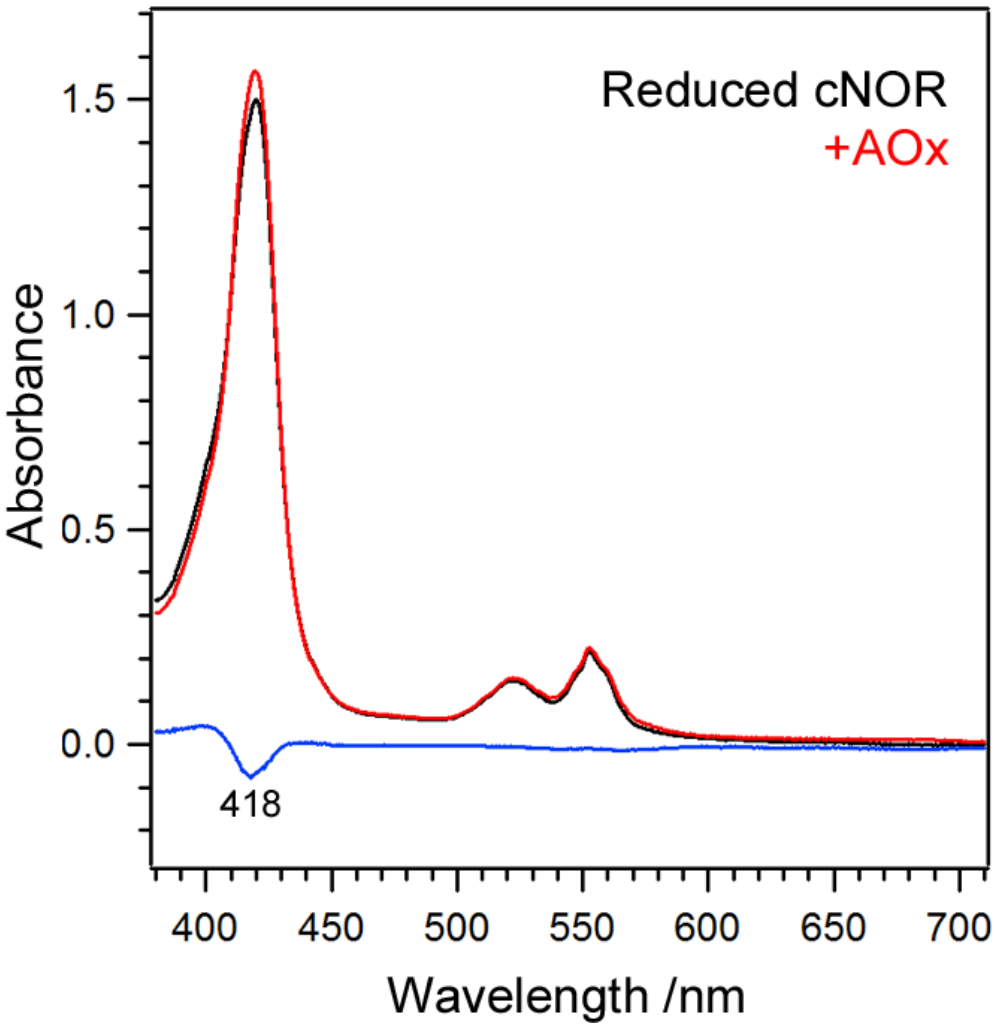

Figure 19. Optical absorption spectra for cNOR. Panel shows optical absorption spectra for the solution state of reduced Ax-bound cNOR. Black and red lines were obtained from reduced cNOR and reduced Ax-bound cNOR, respectively. Blue lines indicate the difference between them. Spectra were obtained in 100 mM sodium citrate, pH 6.0, 50 mM NaCl, and 0.1% *n*-decyl-b-D-thiomaltoside.

I solved the crystal structure of the reduced form of cNOR in the

presence of AOx at a resolution of 2.3 Å. The large positive electron density at the active site in the $F_o - F_c$ map indicates that AOx is located at the binuclear center in cNOR (Fig. 20). To determine the configuration of the AOx binding mode, I constructed several structural models using both the (*E*) and (*Z*) isomers of AOx, because the AOx reagent I used was a regioisomeric mixture. Based on the Raman result showing that the nitrogen atom of AOx coordinates to the heme b_3 iron in cNOR, we carried out crystallographic refinement with a distance restraint of 2.0 Å between the heme b_3 iron and the nitrogen atom of AOx. An (*E*) isomer-bound model provided a reasonable fit to the electron density map (Fig. 20A), which was confirmed by no residual electron density greater than 3 σ in the $F_o - F_c$ map. Similarly, the (*Z*)-isomer of AOx could explain the positive electron density between heme b_3 and Fe_B (Fig. 20B). However, in the best model for the (*Z*) isomer of the AOx-bound form, the methyl group of AOx was located in close proximity to Fe_B (Fig. 20B). Since the (*E*) isomer bound model shows less steric hindrance than that in the (*Z*) isomer bound model, we can therefore suggest that the (*E*) isomer of the AOx-bound form is more likely, although a possibility of the binding of the (*Z*) isomer cannot be completely excluded from current data. In either case, AOx binds to the active site of cNOR, and the nitrogen atom and hydroxyl group of AOx coordinate to the heme b_3 iron and non-heme Fe_B, respectively (heme b_3 Fe-N distance, ~2.0 Å; Fe_B-O distance, 2.0 Å) (Figs. 20). Similar to the CO ligand-bound forms, no notable

structural change was detected in the overall structure, although the Fe-Fe distance increased to 4.4 Å compared with that in oxidized (3.8 Å) or reduced cNOR (4.2 Å), and an additional water molecule near Glu215 was also detected, owing to the improved resolution (Fig. 15). The binuclear active center of NOR can even accommodate a bulky Ax molecule without undergoing any large conformational change such as the dissociation of the amino acid ligands for Fe_B.

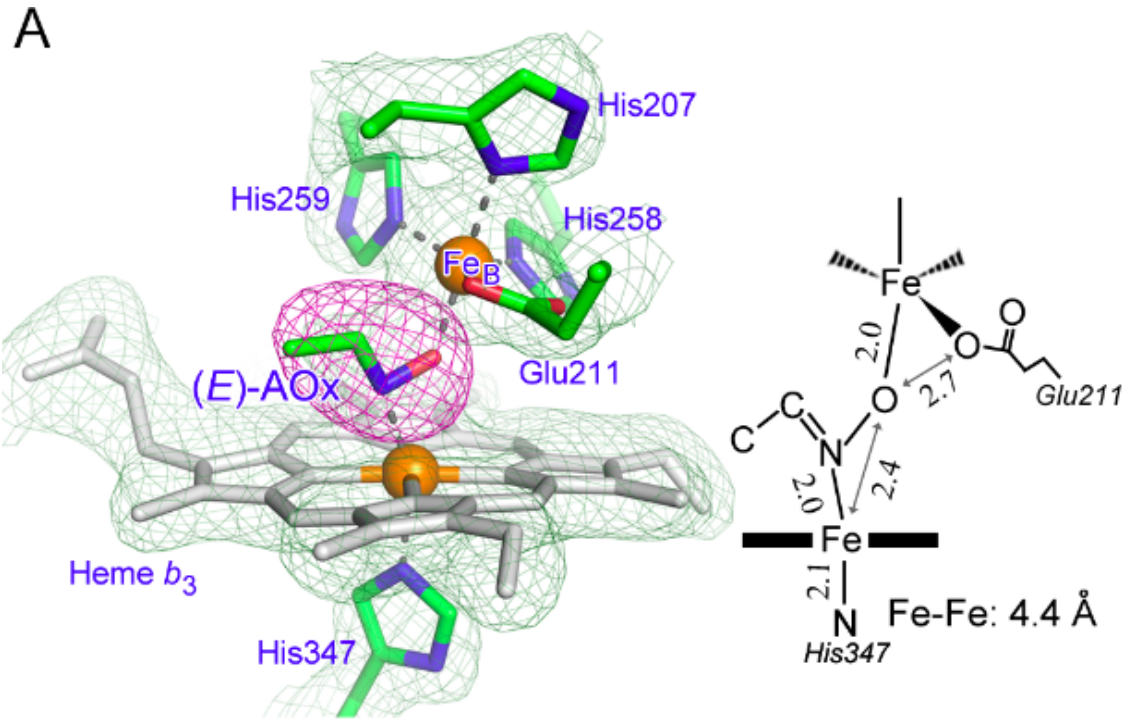

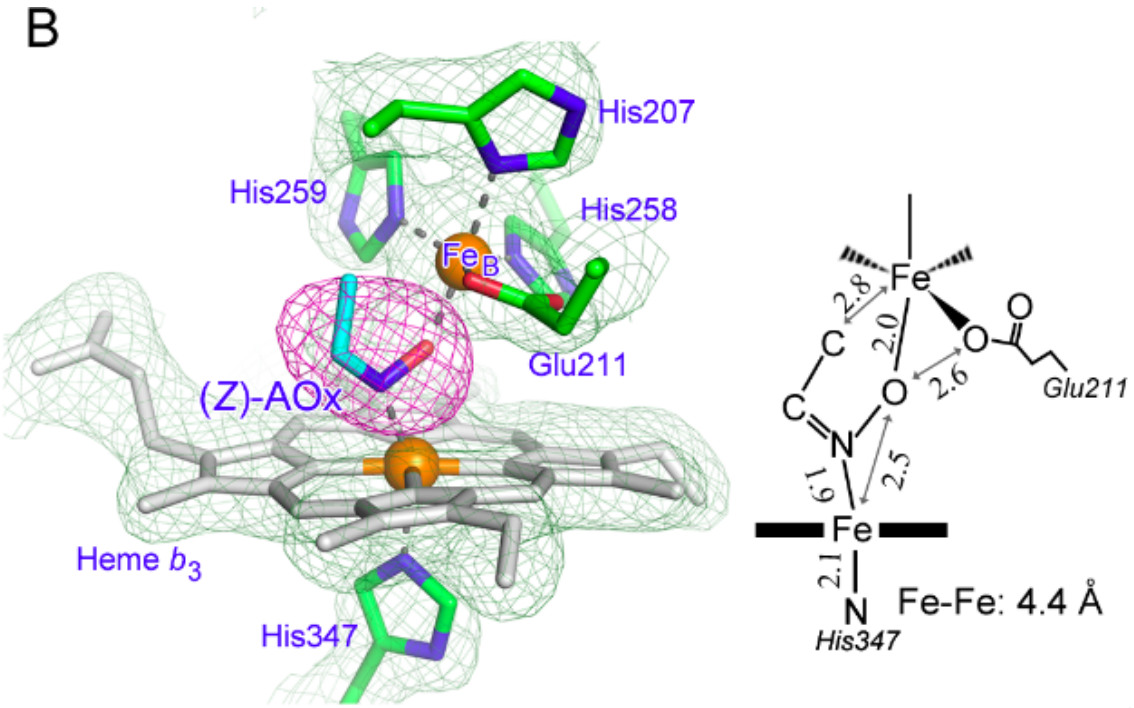

Figure 20. Structures of NO reduction site of the reduced and Ax-bound forms of *P. aeruginosa* cNOR. *Light green mesh* represents the $2F_o - F_c$ electron density map for the binuclear center at 1.2σ for Ax-bound cNOR. Structural characteristics at the binuclear active center are indicated as schematic representations. Panels (A) and (B) represent the binuclear center of reduced (*E*) isomer of Ax-bound model and (*Z*) isomer bound model, respectively. The $F_o - F_c$ map (*magenta mesh*) contoured at 6σ indicates the binding of Ax. The (*E*) isomer of Ax-bound form would be more plausible since the (*E*) isomer bound structure shows less steric hindrance as compared with the (*Z*) isomer bound model.

DISCUSSION

Lack of redo and ligand binding induced conformational changes in cNOR

In the present study, I examined the protein conformational changes in *P. aeruginosa* cNOR as a function of the reduction of iron and ligand binding at the active site, since it has been suggested that redo-dependent conformational changes are crucial for proton pumping coupled with catalytic O_2 reduction in CCO. Reduction of the binuclear center induced significant structural changes in the proton transfer pathway(s) as well as in the active sites for bovine and bacterial aa_3 CCO (A-type CCO) (Ferguson-Miller *et al.*, 2012; Matsumoto *et al.*, 2012; Qin *et al.*, 2009; Tsukihara *et al.*, 2003; Yoshikawa *et al.*, 1998; Yoshikawa *et al.*, 2006). Both bovine and bacterial *R. sphaeroides* aa_3 CCO showed redo-dependent conformational changes of the protein in a helix located between heme *a* and a_3, called helix X (Qin *et al.*, 2009; Tsukihara *et al.*, 2003) (Fig. 22B), which was suggested to be a gating function for the proton-pumping activity in A-type CCO. For example, in bovine aa_3 CCO, the conformational change of helix X induces the orientation change of Ser382 (Fig. 22B), and evokes the open/close of a water channel involved in putative proton pumping pathway, which likely tunes the timing of proton transfer and suppresses proton backflow (Muramoto *et al.*, 2010). Very recently, time-resolved infrared

spectroscopic analysis revealed that the conformational change of helix X was observed even in the solution state of bovine aa_3 CCO, and suggested the relationship with the proton pumping function (Kubo *et al.*, 2013). However, no such redo-induced structural change at the helix X region and presumed proton transfer pathways were detected in cNOR as shown in Fig. 22A, indicating that cNOR and CCO have different structural and functional properties in response to redo change.

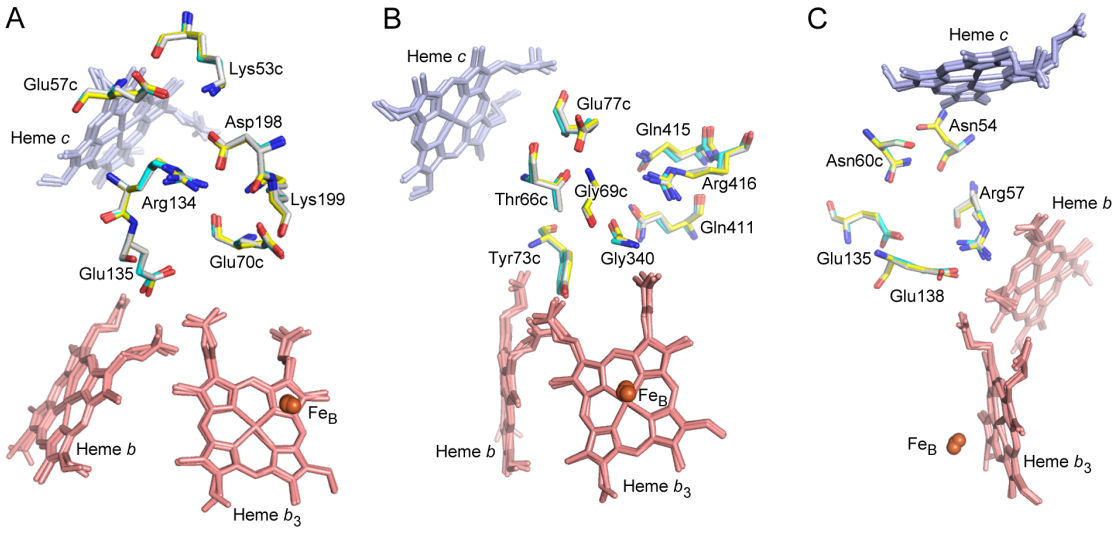

Figure 21. No remarkable structural change in the presumed proton transfer pathways and are evident in cNOR. Panels (A), (B), and (C) show the channel 1, 2, and 3 (presumed proton transfer pathways) regions, respectively, in the superposed structures of oxidized (*yellow*), reduced (*cyan*), and reduced CO-bound (*white*) cNOR.

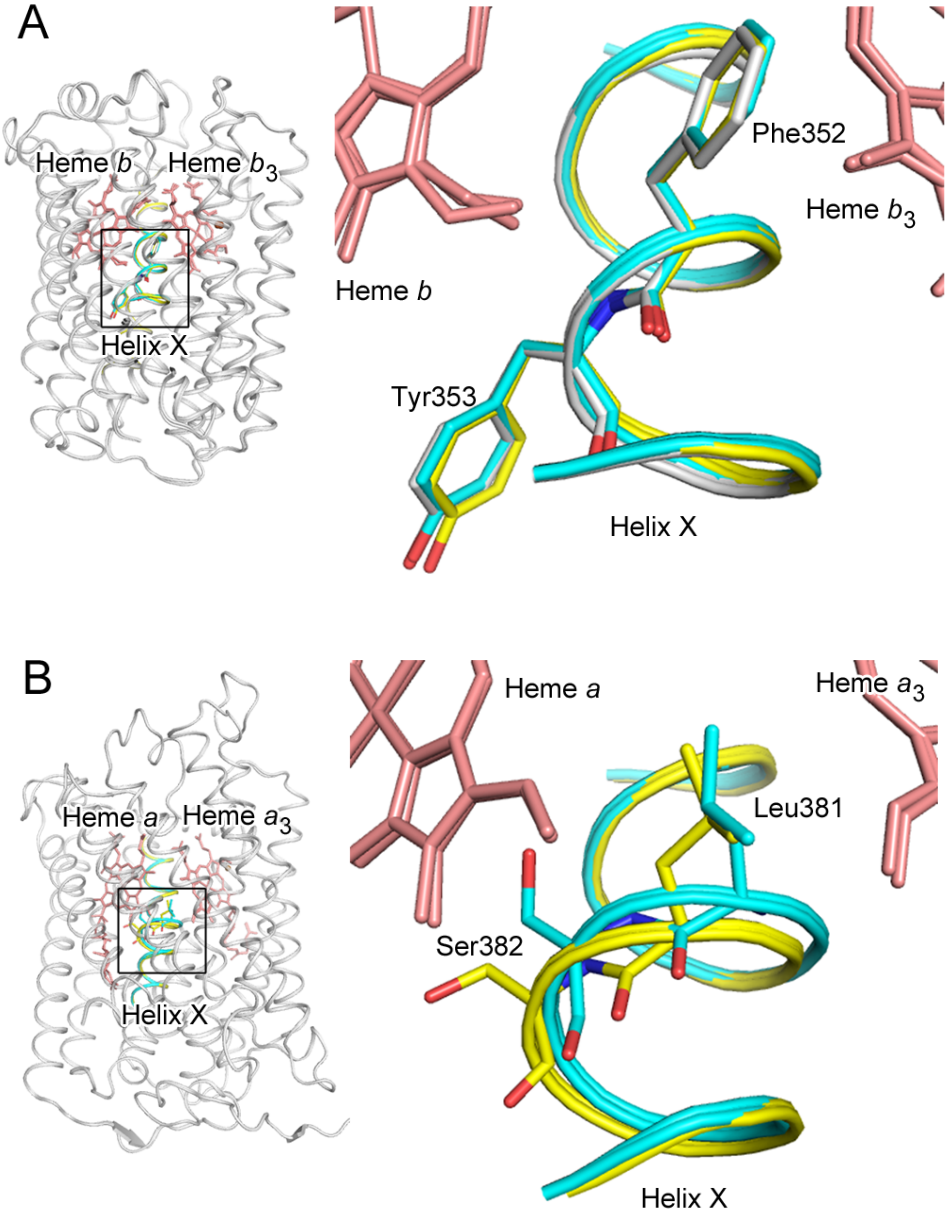

Figure 22. No remarkable structural change in Helix X is evident in cNOR. Panel (A) shows helix X sandwiched by heme *b* and heme b_3 in the superposed structures of oxidized (yellow), reduced (cyan), and reduced CO-bound (white) cNOR. Panel (B) shows a conformational change in helix X of bovine aa_3 COX upon reduction. *Yellow* and *cyan* structures show the oxidized and reduced forms, respectively.

In spite of the slight but further increase in the Fe-Fe distance in the ligand-bound form (4.4 Å) compared to the reduced form of cNOR (4.2 Å) (Table 3), ligand binding to the binuclear center in cNOR also failed to induce any structural changes in the potential proton transfer pathway(s) and helix X sandwiched between heme *b* and heme b_3 (Fig. 21). The absence of any structural change other than active site, even though the change in the Fe-Fe distance by the reduction and ligand binding (~0.5 Å) is larger or comparable as compared with those in Coos (Table 3), suggests that no signal transduction pathway between the binuclear active center and other parts of the protein exist in cNOR. cNOR shows no proton pumping activity during the catalytic reaction and thus does not need to regulate the timing and backflow of catalytic proton transfer. Therefore, my observation that cNOR shows only very localized structural changes in response to redo change and ligand binding at the binuclear center is reasonable. In addition, this view is consistent with the fact that the rapid decomposition of cytotoxic NO produced from the reduction of nitrite NO_2^- by nitrite reductase is a required step in the denitrification process.

Table 3. Heme iron : non-heme metal distances in the respiratory enzymes.

Protein	Oxidation state (ligand)	PDB ID	Distance (Å)	ref
NOR				
cNOR (*P. aeruginosa*)	Oxidized (oxo)	3O0R	3.8	(Hino *et al.*, 2010)
cNOR (*P. aeruginosa*)	Reduced	3WFB	4.2	This study
cNOR (*P. aeruginosa*)	Reduced CO	3WFC	4.4	This study
cNOR (*P. aeruginosa*)	Reduced AOx	3WFE	4.4	This study
CCO				
aa_3 (*Bovine*)	Oxidized (peroxo)	2ZXW	4.9	(Aoyama *et al.*, 2009)
aa_3 (*Bovine*)	Oxidized (nothing)	1V54	5.0	(Tsukihara *et al.*, 2003)
aa_3 (*Bovine*)	Reduced (nothing)	1V55	5.1	(Tsukihara *et al.*, 2003)
aa_3 (*Bovine*)	Reduced (nothing)	2EIJ	5.2	(Muramoto *et al.*, 2007)
aa_3 (*Bovine*)	Reduced CN	3AG4	5.0	(Muramoto *et al.*, 2010)
aa_3 (*Bovine*)	Reduced CO	1OCO	5.4	(Yoshikawa *et al.*, 1998)
aa_3 (*R. sphaeroides*)	Oxidized (H_2O + OH^-)	1M56	4.8	(Svensson-Ek *et al.*, 2002)
aa_3 (*R. sphaeroides*)	Reduced (nothing)	3FYE	5.3	(Qin *et al.*, 2009)
aa_3 (*R. sphaeroides*)	Reduced CN	3FYI	5.0	(Qin *et al.*, 2009)
ba_3 (*T. thermophilus*)	Oxidized (H_2O)	1XME	4.4	(Hunsicker-Wang *et al.*, 2005)
ba_3 (*T. thermophilus*)	Oxidized (peroxo)	3S8F	4.9	(Tiefenbrunn *et al.*, 2011)
ba_3 (*T. thermophilus*)	Reduced (nothing)	3EH3	5.1	(Liu *et al.*, 2009)
ba_3 (*T. thermophilus*)	Reduced (nothing)	3EH4	4.7	(Liu *et al.*, 2009)
ba_3 (*T. thermophilus*)	Reduced (nothing)	3EH5	5.0	(Liu *et al.*, 2009)
ba_3 (*T. thermophilus*)	Reduced CO	3QJQ	5.1	(Liu *et al.*, 2012)

Active site structures of ligand-bound cNOR

For an understanding of the reaction mechanism of NOR at the atomic level, structural information for the ligand-bound forms is urgently needed. In the present study, even though the electron density was obtained at a medium resolution (~2.5 Å), we are in position to propose possible models of the CO-bound cNOR, in which a total of four atoms, e.g. two CO molecules or one CO plus two water molecules, could be accommodated in the binuclear active center in cNOR, on the basis of the comprehensive refinement with various possible models. To get insights into the active site structure of the CO-bound cNOR, measurements of vibration spectra both in solution and crystalline states would be necessary. The infrared spectrum in solution at ambient temperature showed single C-O stretching mode at 1972 cm^{-1}, which is also observed in the resonance Raman spectrum (data not shown). The current data suggests that only a single CO molecule may bind to heme b_3 iron at the binuclear center in the solution. For better characterization of the active site, it is desirable to measure the spectrum under the same conditions during X-ray crystallography experiments; i.e., the presence of precipitant (30% PEG400) at 100 K. However, the presence of high concentration of PEG400 induced precipitation of cNOR, which hampered spectroscopic measurement. We are currently developing a microscopic infrared system applicable to crystalline samples to further characterize the structure of the binuclear center in the CO-bound cNOR.

While we could not determine the binding mode of the CO ligand(s) in the binuclear center, the proposed model for the CO-bound form appears to be consistent with our finding that the binuclear active center of cNOR can accommodate a bulky molecule, namely, Ax: CH_3-CH=N-OH. In addition, Moënne-Loccoz and co-workers observed two CO stretching vibrations at 1972 and 2068 cm^{-1} in an IR study of *Bacillus azotoformans* qCu_ANOR (which is an analogous NOR, but with a dicopper site in the hydrophilic domain as an electron mediator for NO reduction from both cytochrome *c* and quinol) (Lu *et al.*, 2004). This spectroscopic result suggested that two CO molecules could simultaneously coordinate to heme b_3 and Fe_B in qCu_ANOR (Lu *et al.*, 2004). Since only a single diatomic ligand was observed in the heme/Cu_B binuclear center of the ligand- (CO, CN and NO) bound CCO (Liu *et al.*, 2012; Muramoto *et al.*, 2010; Tsukihara *et al.*, 2003), it is noteworthy that binding of total of four atoms, possibly two CO molecules, to the binuclear active center constitute unique structural and functional features in cNOR, but not in evolutionary and structurally related CCO.

The proposed structures of the active sites of the ligand-bound forms of cNOR are consistent with the structural properties required for catalytic NO reduction. In all of the proposed mechanisms for the reduction of NO by NOR (Blomberg & Siegbahn, 2012; Collman *et al.*, 2008; Kumita *et al.*, 2004; Moenne-Loccoz, 2007; Timoteo *et al.*, 2011), two NO molecules must be accommodated at the binuclear center. Therefore, NOR requires

structural characteristics for two NO molecules to bind at the active site. As a possible structural aspect, we can simply expect that NOR has a larger space than CCO, in which only a single O_2 molecule binds to the active site during catalysis. Nevertheless, the coordination sphere around Fe_B is crowded and the Fe-Fe distance is relatively short (3.8 Å) in the resting state of cNOR as compared with the Fe-Cu distance of ~5 Å in CCO (Table 3). It was, therefore, suggested that some conformational changes are needed in order to accommodate two NO molecules (Hino *et al.*, 2012; Shiro, 2012). Indeed, in the structure of *G. stearothermophilus* qNOR in which Fe_B was accidentally replaced with Zn in the crystal preparation, the metal replacement caused the dissociation of the conserved Glu from the non-heme metal to give an active site space larger than that in cNOR (Matsumoto *et al.*, 2012). The qNOR structure suggests that the dissociation of the Glu ligand (Glu211 in *P. aeruginosa* cNOR) from Fe_B is a plausible structural change that would allow two NO molecules to be accommodated at the active site (Shiro, 2012; Tosha & Shiro, 2013). However, the dissociation of Glu211 from Fe_B was never observed in the reduced and reduced ligand-bound cNOR in the present study (Figs. 11 and 14). The 0.5 Å increase in Fe-Fe distance without the dissociation of the Glu ligand from Fe_B permits Ax and possibly two CO molecules to be accommodated at the binuclear center (Figs. 14 and 20). The recent theoretical study of cNOR also showed that the coordination of Glu211 to Fe_B was intact during the catalytic reaction, while the reaction

intermediate with two NO molecules with an increase in Fe-Fe distance to ~4.8 Å was predicted (Blomberg & Siegbahn, 2012). The dissociation of the Glu ligand from Fe_B is unlikely to be an essential factor in accommodating two molecules, although the dissociation of Glu by prolongation of the carboxylate side chain might be involved in proton transfer to the active site, as has been previously proposed (Shiro, 2012; Tosha & Shiro, 2013).

To elucidate the structural basis of a total of four atoms, e.g. two CO molecules, or Ax, binding in cNOR, we carried out a detailed examination of the active site. As shown in Figure 23, cNOR has a hydrophobic space next to the binuclear active center, which is not observed in the A-type CCO. In contrast to CCO, possibly two CO molecules or Ax could be accommodated at the binuclear center in cNOR due to this additional hydrophobic space. This hydrophobic space, which is characteristic in cNOR could be important in the simultaneous binding of two NO substrates for the NO reduction reaction. Comparing the amino acid residues that create the hydrophobic pocket in cNOR with those of Coos provides further insights into the structural properties required for the NO reducing reaction. Trp203, Val206, and Val210, which are highly conserved in NORs, constitute this hydrophobic heme pocket (Figs. 23 and 25). Interestingly, although Trp203 and Val210 are conserved even in Coos, Val206 is replaced with a smaller residue, namely, Gly or Ser (only a subfamily of A-type CCO, classified as type A2, contains a Ser at this position (Pereira *et al.*, 2001)) (Fig. 25). Val206 could

likely play a vital role in suppressing the escape of the ligand (substrate) from the heme pocket to the outside of the protein in cNOR. This view is in reasonably good agreement with the much faster rebinding of CO or NO, namely, geminate recombination, to heme b_3 iron in *Pa. denitrificans* cNOR compared to CCO (Kapetanaki *et al.*, 2008; Pisliakov *et al.*, 2012). These structural properties which are unique to cNOR could permit the two NO molecules to remain in the heme pocket for NO reducing reaction.

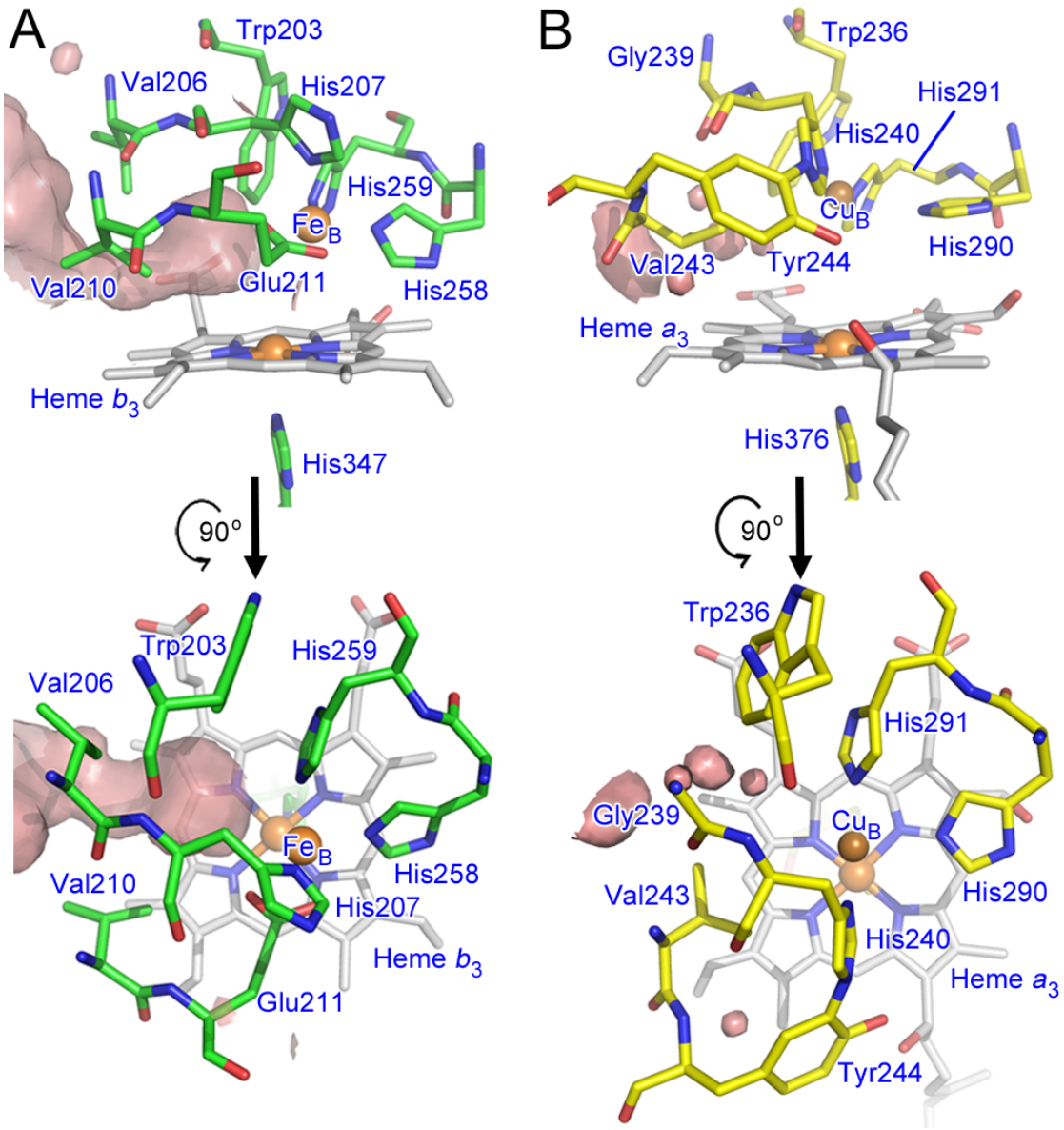

Figure 23. Structure properties responsible for the NOR-catalyzed reaction. Panels (A) and (B) show the active sites of cNOR and A-type bovine aa_3 CCO (PDB ID: 3AG4), respectively. The surfaces represent the active site cavity, and were calculated with a probe radius of 1.0 Å using VOIDOO (Kleywegt & Jones, 1994).

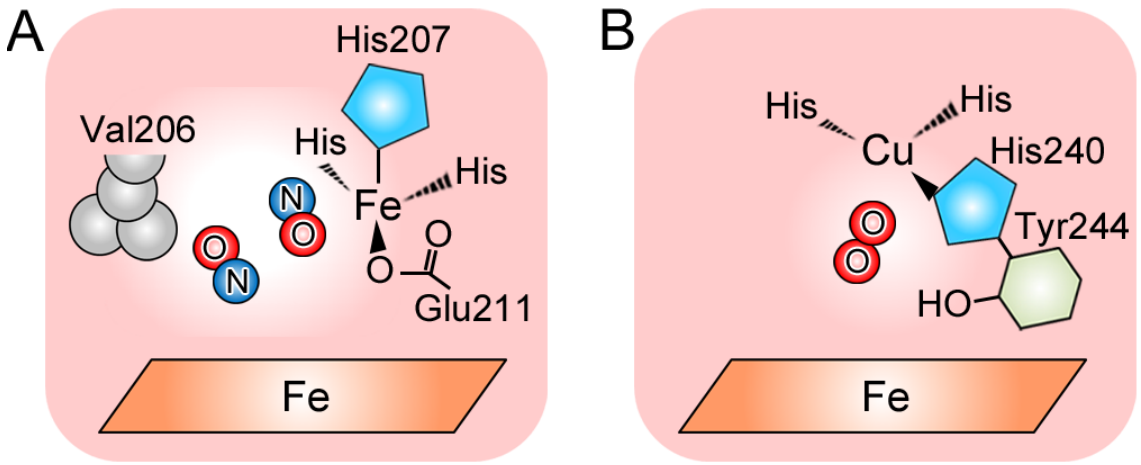

Figure 24. Presumed models of the active site with substrates. Panels (A) and (B) show the schematic representation of the binuclear active center with substrates for cNOR and CCO, respectively. The substrate-bound structure for cNOR is based on the reduced CO-bound structure. Compared with CCO, cNOR has a larger heme pocket but the non-heme metal is in a more crowded environment.

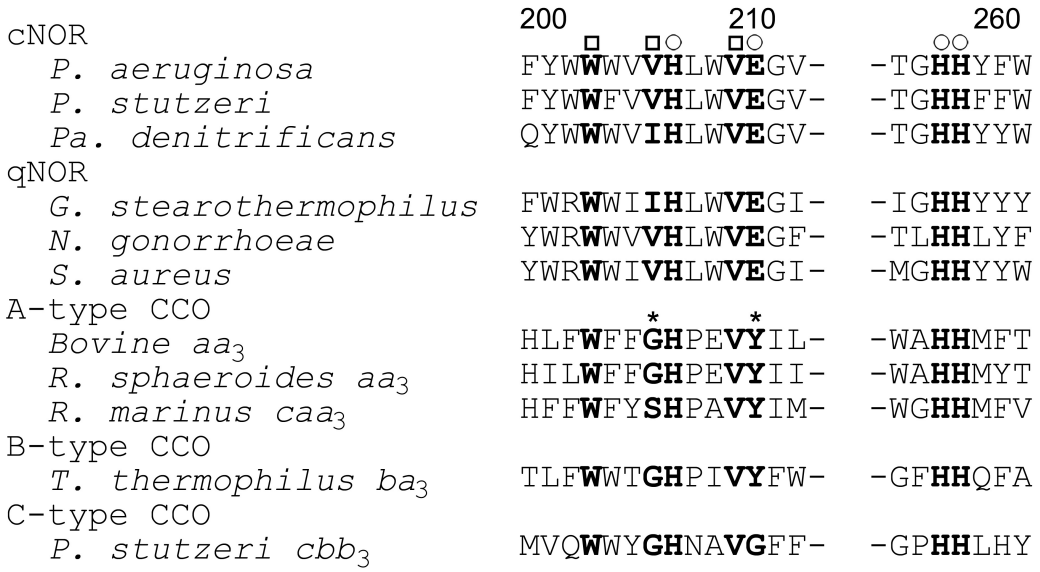

Figure 25. Sequence alignments of the amino acid residues located at the binuclear center of NORs and CCOs. *Circles* indicate the ligands for non-heme metal. *Squares* indicate the residues located at the hydrophobic heme pocket. *Asterisks* indicate the CCO residues that are different from the corresponding residues in NORs. (*P. aeruginosa; Pseudomonas aeruginosa, P. stutzeri; Pseudomnas stutter; Pa. denitrificans; Paracoccus denitrificans, G. stearothermophilus; Geobacillus stearothermophilus, N. gonorrhoeae; Neisseria gonorrhoeae, S. aureus; Staphylococcus aureus, R. sphaeroides; Rhodobacter sphaeroides, R. marinus; Rhodothermus marinus, T. thermophilus; Thermus thermophilus*)

Note that, despite the potential presence of two CO molecules or a bulky Ax at the active site in the ligand-bound cNOR, the Fe-Fe distance in the ligand-bound forms (~4.5 Å) is shorter than that in CCO (~5 Å), in which a single diatomic ligand such as CO coordinates to the binuclear active center (Table 3). A close inspection of the active site structures suggests that the positional difference of one of the His ligands for non-heme metal between cNOR and CCO likely controls the distance of the heme/non-heme metal bond. A ligand for Fe_B in cNOR, His207, is located on the axis where the heme iron and Fe_B are connected (Fig. 24). Therefore, His207 could serve as a limiter to inhibit the movement of Fe_B away from the heme, even when a bulky ligand is present at the active site. However, the corresponding His (His240 in bovine aa_3 CCO) is located in the plane consisting of Cu_B and the other two His ligands in CCO, and largely deviates from the heme plane, leading to a longer Fe-Cu distance. The active site architecture of cNOR permits the Fe-Fe distance to be shorter than that in CCO. A shorter Fe-Fe distance would enable the two NO molecules to be closer, thus enhancing the efficiency of N-N coupling for the formation of the hyponitrite intermediate during the catalytic reaction by cNOR.

In summary, we solved the crystal structures of the reduced, CO-, and Ax-bound forms of *P. aeruginosa* cNOR. In contrast to CCO, no structural changes in the proton transfer pathways and the helix X region were detected, upon redo change and ligand binding in cNOR, explaining the

lack of a gating function for proton pumping. This finding is consistent with the physiological role of the rapid decomposition of a large amount of cytotoxic NO produced by the reduction of nitrite NO_2^- by nitrite reductase in the denitrification process. We also found that cNOR could accommodate the bulky Ax and probably two CO molecules to the binuclear active center. Because two NO substrates, a total of four atoms, must bind to the active site for the NOR-catalyzed reaction, the structure of CO- and Ax-bound forms are useful in terms of elucidating the structural elements required for the NO reducing reaction. The ligand-bound structures suggest that only a ~0.5 Å increase in the Fe-Fe distance allows two NO substrates to bind at the active site, and allows two NO molecules to be maintained within a short distance for effective N-N coupling. Further structural studies on short-lived reaction intermediate(s) by time-resolved spectroscopy combined with X-ray crystallography as well as high-resolution structures will help in developing a further understanding of the catalytic mechanism of NO reducing reaction.

Chapter 4

General conclusion

Nitric oxide reductase (NOR) is an integral membrane protein that is involved in microbial denitrification, a type of anaerobic respiration in which nitrate is reduced in a stepwise manner to dinitrogen ($NO_3^- \rightarrow NO_2^- \rightarrow NO \rightarrow N_2O \rightarrow N_2$). NOR catalyzes the generation of nitrous oxide (N_2O) via the reductive coupling of two nitric oxide (NO) molecules at a heme/non-heme Fe center. The elucidation of the mechanism of the NOR-catalyzed reaction is highly desirable because N_2O produced by NOR is a powerful global warming gas in the ecological nitrogen cycle. I therefore tried to elucidate the molecular mechanism of the NO reducing reaction by NOR. To this purpose, I determined the atomic and molecular structures of NOR in different states involved in the enzymatic reaction cycle. The results obtained from this thesis are summarized below.

To discuss the catalytic mechanism, it is necessary to determine the active site structure of NOR at atomic resolution. However, the highest resolution of the NOR structure reported now is at a medium resolution (2.7 Å). For the purpose of improving the resolution, I re-examined the methods of purification and crystallization of cytochrome *c*-dependent NOR (cNOR) from *Pseudomonas aeruginosa* in chapter 2. I found that the last purification

step by a cation exchange chromatography was effective for purifying homogeneous cNOR. The micro-seeding method used for the crystallization of cNOR guaranteed the reproducibility of the crystal formation and the quality of the crystals. With use of the purification and crystallization methods established here, the resolution was improved from 2.7 Å to ~2.3 Å. Thus, careful evaluation of the method for the sample preparation (including the crystallization) is critical for obtaining crystals with high quality.

Even though the resolution was improved, it is still difficult to determine the atomic structure of the active site of cNOR, in particular the ligand-bound state, due to the presence of two strong scatters, heme b_3 iron and Fe_B. In chapter 2, the analysis method for the active site of cNOR was also established through the structural determination of the cyanide-bound form. I found that comprehensive crystallographic refinement with all possible models was required to construct the model of the active site of cNOR. The structural analysis method developed here can be applied to the other metalloproteins, in which the active site contains multiple metal atoms.

The structural determination of cyanide-bound cNOR in chapter 2 indicated that the reduced form would be a good target for the structural analysis of the ligand-bound state, since ligand binding requires the dissociation of oxo-ligand in the oxidized state, which causes the presence of ligand-bound and ligand-free (oxo-bound) forms in the crystal structure. In

chapter 3, I therefore tried to solve the crystal structures of the reduced, CO-, and AOx-bound forms of *P. aeruginosa* cNOR. The main findings from the structures of the ligand-bound forms are that cNOR could accommodate the bulky AOx (CH_3-CH=N-OH) and probably two CO molecules to the binuclear active center. Since two NO substrates, equivalent to a total of four atoms, must bind to the active site in the short lived intermediate for the NOR-catalyzed reaction, the structure of CO- and AOx-bound forms are useful as a model for elucidating the coordination structure at the active site of the intermediate. From the observation that the binding of CO or AOx to cNOR induced only a ~0.5 Å increase in the Fe-Fe distance, we can conclude that cNOR allows two NO substrates to bind to the active site, and allows two NO molecules to be maintained within a short distance for effective N-N coupling.

Comparing the results obtained from the structural analysis on cNOR with those of CCO also provides insights into the structural elements required for the respective function of the respiratory enzymes. In contrast to CCO, except for the active site no structural changes in the proton transfer pathways or the other parts of the protein were detected upon redox change and ligand binding in cNOR, explaining the lack of a gating function for proton pumping. This finding is consistent with the physiological role of the rapid decomposition of a large amount of cytotoxic NO produced by the reduction of nitrite NO_2^- by nitrite reductase in the denitrification process.

cNOR would enable the quick NO detoxication without prominent structural changes which requires extra energy.

In summary, this thesis provides methods for X-ray crystal structural analysis of the binuclear center of NOR and the structural basis responsible for the catalytic NO reduction. However, for a complete understanding of the catalytic mechanism of NO reducing reaction, further structural characterizations on short-lived reaction intermediate(s) by more advanced structural study, such as a combination of a pump-probe experiment with silial femtosecond crystallography performed at X-ray free electron laser (XFEL), are required. I believe that the technique established in this thesis should be applicable to new technologies and useful for the structural determination of the active site of cNOR in reaction intermediate(s). Understanding the mechanism of the generation of N_2O, a powerful greenhouse gas, generation by NOR will fascinate not only chemists but also environmental scientists. Furthermore, the structural information on NOR could probably help design novel anti-bacterial drugs since some pathogenic bacteria including *P. aeruginosa* utilize NOR to decompose the NO produced from the host's immune system. I hope that the findings obtained through this thesis will contribute to the development of fundamental chemistry, in particular bioinorganic chemistry, and will be useful for environmental, pharmaceutical and medical studies.

Acknowledgements

This thesis would not have been possible without the kind support and encouragement of many people. First of all, I am very grateful to Professor Yoshihiko Sako, my supervisor, for giving me the opportunity to try new fields of study. I couldn't have spent all of the seven years for exciting study without his warm advice and encouragements. I also thank Dr. Takashi Yoshida, and Dr. Shigeki Sawayama for reviewing my thesis.

I can never thank enough Dr. Yoshitsugu Shiro, my supervisor in RIKEN, for accepting me as a junior research associate in RIKEN. He taught me the fascinating world of the research on bioinorganic chemistry and led me to the point of viewing world standards of science. I am also very grateful to Dr. Takehiko Tosha (RIKEN) for teaching me how to study bioinorganic chemistry and express results to the world. I have learned a lot of details and important things about being a scientist from him. I am also very grateful to Dr. Hiroshi Sugimoto (RIKEN) for teaching me the world of X-ray crystallography and the technique of structural analysis. I wouldn't have been able to get any structural data without his skills and comprehensive knowledge of X-ray crystal structure analysis. I am also very grateful to Dr. Tomoya Hino (Tottori University) for teaching me how to purify and crystallize difficult membrane proteins. His enthusiasm and love for studying membrane protein encouraged me to learn about this field that was

new and difficult for me.

I thank S. Ishii (University of Hyogo) and K. Takatsu (RIKEN) for their support in sample preparation and the staff of the SPring-8 beam-lines for their help with diffraction measurements and micro-photometry. The diffraction expesiments were performed at SPring-8 BL41XU (Proposals 2010B1618, 2011A1520, 2011B1603, 2012A1478 and 2012B1526). I also thank Prof. T. Ogura (University of Hyogo) for kindly permitting us to use his Raman equipment.

I was supported by a grant-in-aid for junior research associates of RIKEN.

On a more personal note, I could never have reached today without the support of my family and friends. I thank every one who gave me a lot of love, support, patience and encouragement.

References

Aoyama H, Muramoto K, Shinzawa-Itoh K, Hirata K, Yamashita E, Tsukihara T, Ogura T, Yoshikawa S (2009). A peroxide bridge between Fe and Cu ions in the O_2 reduction site of fully oxidized cytochrome c oxidase could suppress the proton pump. *Proc Natl Acad Sci U S A* **106**, 2165-2169.

Blomberg MR, Siegbahn PE (2012). Mechanism for N_2O generation in bacterial nitric oxide reductase: a quantum chemical study. *Biochemistry* **51**, 5173-5186.

Bueno E, Mesa S, Bedmar EJ, Richardson DJ, Delgado MJ (2012). Bacterial adaptation of respiration from oxic to microoxic and anoxic conditions: redox control. *Antioxid Redox Signal* **16**, 819-852.

Chiu YC, Okajima T, Murakawa T, Uchida M, Taki M, Hirota S, Kim M, Yamaguchi H, Kawano Y, Kamiya N, Kuroda S, Hayashi H, Yamamoto Y, Tanizawa K (2006). Kinetic and structural studies on the catalytic role of the aspartic acid residue conserved in copper amine oxidase. *Biochemistry* **45**, 4105-4120.

Collman JP, Dey A, Yang Y, Decreau RA, Ohta T, Solomon EI (2008). Intermediates involved in the two electron reduction of NO to N_2O by a functional synthetic model of heme containing bacterial NO reductase. *J Am Chem Soc* **130**, 16498-16499.

Ducluzeau AL, van Lis R, Duval S, Schoepp-Cothenet B, Russell MJ, Nitschke W (2009). Was nitric oxide the first deep electron sink? *Trends Biochem Sci* **34**, 9-15.

Emsley P, Cowtan K (2004). Coot: model-building tools for molecular

graphics. *Acta Crystallogr D Biol Crystallogr* **60**, 2126-2132.

Fabian M, Jancura D, Palmer G (2004). Two sites of interaction of anions with cytochrome a in oxidized bovine cytochrome c oxidase. *J Biol Chem* **279**, 16170-16177.

Ferguson-Miller S, Hiser C, Liu J (2012). Gating and regulation of the cytochrome c oxidase proton pump. *Biochim Biophys Acta* **1817**, 489-494.

Flock U, Thorndycroft FH, Matorin AD, Richardson DJ, Watmough NJ, Adelroth P (2008). Defining the proton entry point in the bacterial respiratory nitric-oxide reductase. *J Biol Chem* **283**, 3839-3845.

Girsch P, de Vries S (1997). Purification and initial kinetic and spectroscopic characterization of NO reductase from *Paracoccus denitrificans*. *Biochim Biophys Acta* **1318**, 202-216.

Govan JR, Deretic V (1996). Microbial pathogenesis in cystic fibrosis: mucoid Pseudomonas aeruginosa and *Burkholderia cepacia*. *Microbiol Rev* **60**, 539-574.

Gronberg KL, Watmough NJ, Thomson AJ, Richardson DJ, Field SJ (2004). Redox-dependent open and closed forms of the active site of the bacterial respiratory nitric-oxide reductase revealed by cyanide binding studies. *J Biol Chem* **279**, 17120-17125.

Heiss B, Frunzke K, Zumft WG (1989). Formation of the N-N bond from nitric oxide by a membrane-bound cytochrome bc complex of nitrate-respiring (denitrifying) *Pseudomonas stutzeri*. *J Bacteriol* **171**, 3288-3297.

Hendriks JH, Jasaitis A, Saraste M, Verkhovsky MI (2002). Proton

and electron pathways in the bacterial nitric oxide reductase. *Biochemistry* **41**, 2331-2340.

Hino T, Matsumoto Y, Nagano S, Sugimoto H, Fukumori Y, Murata T, Iwata S, Shiro Y (2010). Structural basis of biological N_2O generation by bacterial nitric oxide reductase. *Science* **330**, 1666-1670.

Hino T, Nagano S, Sugimoto H, Tosha T, Shiro Y (2012). Molecular structure and function of bacterial nitric oxide reductase. *Biochim Biophys Acta* **1817**, 680-687.

Hunsicker-Wang LM, Pacoma RL, Chen Y, Fee JA, Stout CD (2005). A novel cryoprotection scheme for enhancing the diffraction of crystals of recombinant cytochrome ba3 oxidase from *Thermus thermophilus*. *Acta Crystallogr D Biol Crystallogr* **61**, 340-343.

Ju LK, Chen F, Xia Q (2005). Monitoring microaerobic denitrification of *Pseudomonas aeruginosa* by online NAD(P)H fluorescence. *J Ind Microbiol Biotechnol* **32**, 622-628.

Kakishima K, Shiratsuchi A, Taoka A, Nakanishi Y, Fukumori Y (2007). Participation of nitric oxide reductase in survival of *Pseudomonas aeruginosa* in LPS-activated macrophages. *Biochem Biophys Res Commun* **355**, 587-591.

Kapetanaki SM, Field SJ, Hughes RJ, Watmough NJ, Liebl U, Vos MH (2008). Ultrafast ligand binding dynamics in the active site of native bacterial nitric oxide reductase. *Biochim Biophys Acta* **1777**, 919-924.

Kitagawa T (1988). Heme Protein Structure and the Iron-Histidine Stretching Mode. In *Biological Applications of Raman Spectroscopy*, pp. 97-131. Edited by T. G. Spiro. New York: John Wiley & Sons.

Kleywegt GJ, Jones TA (1994). Detection, delineation, measurement and display of cavities in macromolecular structures. *Acta Crystallogr D Biol Crystallogr* **50**, 178-185.

Koepke J, Olkhova E, Angerer H, Muller H, Peng G, Michel H (2009). High resolution crystal structure of *Paracoccus denitrificans* cytochrome c oxidase: new insights into the active site and the proton transfer pathways. *Biochim Biophys Acta* **1787**, 635-645.

Kubo M, Nakashima S, Yamaguchi S, Ogura T, Mochizuki M, Kang J, Tateno M, Shinzawa-Itoh K, Kato K, Yoshikawa S (2013). Effective pumping proton collection facilitated by a copper site (Cu_B) of bovine heart cytochrome c oxidase, revealed by a newly developed time-resolved infrared system. *J Biol Chem* **288**, 30259-30269.

Kumita H, Matsuura K, Hino T, Takahashi S, Hori H, Fukumori Y, Morishima I, Shiro Y (2004). NO reduction by nitric-oxide reductase from denitrifying bacterium *Pseudomonas aeruginosa*: characterization of reaction intermediates that appear in the single turnover cycle. *J Biol Chem* **279**, 55247-55254.

Lee HJ, Reimann J, Huang Y, Adelroth P (2012). Functional proton transfer pathways in the heme-copper oxidase superfamily. *Biochim Biophys Acta* **1817**, 537-544.

Liu B, Chen Y, Doukov T, Soltis SM, Stout CD, Fee JA (2009). Combined microspectrophotometric and crystallographic examination of chemically reduced and X-ray radiation-reduced forms of cytochrome ba3 oxidase from *Thermus thermophilus*: structure of the reduced form of the enzyme. *Biochemistry* **48**, 820-826.

Liu B, Zhang Y, Sage JT, Soltis SM, Doukov T, Chen Y, Stout CD, Fee JA (2012). Structural changes that occur upon photolysis of the Fe(II)

$_{a3}$-CO complex in the cytochrome ba$_3$-oxidase of *Thermus thermophilus*: a combined X-ray crystallographic and infrared spectral study demonstrates CO binding to Cu$_B$. *Biochim Biophys Acta* **1817**, 658-665.

Lovell SC, Davis IW, Arendall WB, 3rd, de Bakker PI, Word JM, Prisant MG, Richardson JS, Richardson DC (2003). Structure validation by Calpha geometry: phi,psi and Cbeta deviation. *Proteins* **50**, 437-450.

Lu S, Suharti, de Vries S, Moenne-Loccoz P (2004). Two CO molecules can bind concomitantly at the diiron site of NO reductase from *Bacillus azotoformans*. *J Am Chem Soc* **126**, 15332-15333.

Matsumoto Y, Tosha T, Pisliakov AV, Hino T, Sugimoto H, Nagano S, Sugita Y, Shiro Y (2012). Crystal structure of quinol-dependent nitric oxide reductase from *Geobacillus stearothermophilus*. *Nat Struct Mol Biol* **19**, 238-245.

Moenne-Loccoz P, de Vries S (1998). Structural characterization of the catalytic high-spin heme *b* of nitric oxide reductase: A resonance Raman study. *J Am Chem Soc* **120**, 5147-5152.

Moenne-Loccoz P (2007). Spectroscopic characterization of heme iron-nitrosyl species and their role in NO reductase mechanisms in diiron proteins. *Nat Prod Rep* **24**, 610-620.

Muramoto K, Hirata K, Shinzawa-Itoh K, Yoko-o S, Yamashita E, Aoyama H, Tsukihara T, Yoshikawa S (2007). A histidine residue acting as a controlling site for dioxygen reduction and proton pumping by cytochrome c oxidase. *Proc Natl Acad Sci U S A* **104**, 7881-7886.

Muramoto K, Ohta K, Shinzawa-Itoh K, Kanda K, Taniguchi M, Nabekura H, Yamashita E, Tsukihara T, Yoshikawa S (2010).

Bovine cytochrome c oxidase structures enable O_2 reduction with minimization of reactive oxygens and provide a proton-pumping gate. *Proc Natl Acad Sci U S A* **107**, 7740-7745.

Ogura T, Takahashi S, Hirota S, Shinzawaitoh K, Yoshikawa S, Appelman EH, Kitagawa T (1993). Time-resolved resonance raman elucidation of the pathway for dioxygen reduction by cytochrome c oxidase. *J Am Chem Soc* **115**, 8527-8536.

Oinuma K, Kumita H, Ohta T, Konishi K, Hashimoto Y, Higashibata H, Kitagawa T, Shiro Y, Kobayashi M (2005). Stopped-flow spectrophotometric and resonance Raman analyses of aldoxime dehydratase involved in carbon-nitrogen triple bond synthesis. *FEBS Lett* **579**, 1394-1398.

Otwinowski Z, Minor W (1997). Processing of X-ray diffraction data collected in oscillation mode. *Methods Enzymol* **276**, 307-326.

Pereira MM, Santana M, Teixeira M (2001). A novel scenario for the evolution of haem-copper oxygen reductases. *Biochim Biophys Acta* **1505**, 185-208.

Pisliakov AV, Hino T, Shiro Y, Sugita Y (2012). Molecular dynamics simulations reveal proton transfer pathways in cytochrome c-dependent nitric oxide reductase. *PLoS Comput Biol* **8**, e1002674.

Qin L, Liu J, Mills DA, Proshlyakov DA, Hiser C, Ferguson-Miller S (2009). Redox-dependent conformational changes in cytochrome c oxidase suggest a gating mechanism for proton uptake. *Biochemistry* **48**, 5121-5130.

Ravishankara AR, Daniel JS, Portmann RW (2009). Nitrous oxide (N_2O): the dominant ozone-depleting substance emitted in the 21st century. *Science* **326**, 123-125.

Reimann J, Flock U, Lepp H, Honigmann A, Adelroth P (2007). A pathway for protons in nitric oxide reductase from *Paracoccus denitrificans*. *Biochim Biophys Acta* **1767**, 362-373.

Richardson D, Felgate H, Watmough N, Thomson A, Baggs E (2009). Mitigating release of the potent greenhouse gas N_2O from the nitrogen cycle could enzymic regulation hold the key? *Trends Biotechnol* **27**, 388-397.

Ridgway HF, Safarik J, Phipps D, Carl P, Clark D (1990). Identification and catabolic activity of well-derived gasoline-degrading bacteria from a contaminated aquifer. *Appl Environ Microbiol* **56**, 3565-3575.

Saraste M, Castresana J (1994). Cytochrome oxidase evolved by tinkering with denitrification enzymes. *FEBS Lett* **341**, 1-4.

Sawai H, Sugimoto H, Kato Y, Asano Y, Shiro Y, Aono S (2009). X-ray crystal structure of michaelis complex of aldoxime dehydratase. *J Biol Chem* **284**, 32089-32096.

Shiro Y (2012). Structure and function of bacterial nitric oxide reductases: nitric oxide reductase, anaerobic enzymes. *Biochim Biophys Acta* **1817**, 1907-1913.

Sousa FL, Alves RJ, Ribeiro MA, Pereira-Leal JB, Teixeira M, Pereira MM (2012). The superfamily of heme-copper oxygen reductases: types and evolutionary considerations. *Biochim Biophys Acta* **1817**, 629-637.

Stevanin TM, Moir JW, Read RC (2005). Nitric oxide detoxification systems enhance survival of *Neisseria meningitidis* in human macrophages and in nasopharyngeal mucosa. *Infect Immun* **73**, 3322-3329.

Suharti, Strampraad MJ, Schroder I, de Vries S (2001). A novel copper A containing menaquinol NO reductase from *Bacillus azotoformans*. *Biochemistry* **40**, 2632-2639.

Svensson-Ek M, Abramson J, Larsson G, Tornroth S, Brzezinski P, Iwata S (2002). The X-ray crystal structures of wild-type and EQ(I-286) mutant cytochrome c oxidases from *Rhodobacter sphaeroides*. *J Mol Biol* **321**, 329-339.

Tiefenbrunn T, Liu W, Chen Y, Katritch V, Stout CD, Fee JA, Cherezov V (2011). High resolution structure of the ba_3 cytochrome c oxidase from *Thermus thermophilus* in a lipidic environment. *PLoS One* **6**, e22348.

Timoteo CG, Pereira AS, Martins CE, Naik SG, Duarte AG, Moura JJ, Tavares P, Huynh BH, Moura I (2011). Low-spin heme b_3 in the catalytic center of nitric oxide reductase from *Pseudomonas nautica*. *Biochemistry* **50**, 4251-4262.

Tosha T, Shiro Y (2013). Crystal structures of nitric oxide reductases provide key insights into functional conversion of respiratory enzymes. *IUBMB Life* **65**, 217-226.

Tsukihara T, Shimokata K, Katayama Y, Shimada H, Muramoto K, Aoyama H, Mochizuki M, Shinzawa-Itoh K, Yamashita E, Yao M, Ishimura Y, Yoshikawa S (2003). The low-spin heme of cytochrome c oxidase as the driving element of the proton-pumping process. *Proc Natl Acad Sci U S A* **100**, 15304-15309.

Vagin AA, Teplyakov A (1997). MOLREP: an atuomated program for molecular replacement. *J Appl Cryst* **30**, 1022-1025.

Vagin AA, Steiner RA, Lebedev AA, Potterton L, McNicholas S, Long F, Murshudov GN (2004). REFMAC5 dictionary: organization of prior chemical knowledge and guidelines for its use. *Acta Crystallogr D Biol Crystallogr* **60**, 2184-2195.

Vaguine AA, Richelle J, Wodak SJ (1999). SFCHECK: a unified set of procedures for evaluating the quality of macromolecular structure-factor data and their agreement with the atomic model. *Acta Crystallogr D Biol Crystallogr* **55**, 191-205.

van der Oost J, de Boer AP, de Gier JW, Zumft WG, Stouthamer AH, van Spanning RJ (1994). The heme-copper oxidase family consists of three distinct types of terminal oxidases and is related to nitric oxide reductase. *FEMS Microbiol Lett* **121**, 1-9.

Watmough NJ, Field SJ, Hughes RJ, Richardson DJ (2009). The bacterial respiratory nitric oxide reductase. *Biochem Soc Trans* **37**, 392-399.

Wink DA, Hines HB, Cheng RY, Switzer CH, Flores-Santana W, Vitek MP, Ridnour LA, Colton CA (2011). Nitric oxide and redox mechanisms in the immune response. *J Leukoc Biol* **89**, 873-891.

Yi J, Morrow BH, Campbell AL, Shen JK, Richter-Addo GB (2012). Nitric oxide coupling mediated by iron porphyrins: the N-N bond formation step is facilitated by electrons and a proton. *Chem Commun (Camb)* **48**, 9041-9043.

Yoshikawa S, Shinzawa-Itoh K, Nakashima R, Yaono R, Yamashita E, Inoue N, Yao M, Fei MJ, Libeu CP, Mizushima T, Yamaguchi H, Tomizaki T, Tsukihara T (1998). Redox-coupled crystal structural changes in bovine heart cytochrome c oxidase. *Science* **280**, 1723-1729.

Yoshikawa S, Muramoto K, Shinzawa-Itoh K, Aoyama H, Tsukihara T, Shimokata K, Katayama Y, Shimada H (2006). Proton pumping mechanism of bovine heart cytochrome c oxidase. *Biochim Biophys Acta* **1757**, 1110-1116.

Zumft WG (2005). Nitric oxide reductases of prokaryotes with emphasis on the respiratory, heme-copper oxidase type. *J Inorg Biochem* **99**, 194-215.

Publication list

1. **Sato N.**, Ishii S., Sugimoto H, Hino T., Fukumori Y., Sako Y., Shiro Y., and Tosha T. Structures of reduced and ligand-bound nitric oxide reductase provide insights into functional differences in respiratory enzymes. (***Proteins: Structure, Function and Bioinformatics.*** In press, doi: 10.1002/prot.24492)(Chapter 3)

Other publications

1. Tenaska E., Okada N., **Sato N.**, Sako Y., Shire Y., and Tasha T. Characterization of Quinol-dependent Nitric oxide reductase from Geobacillus stearothermophilus: Enzymatic activity and active site structure. (Submitted to ***Biochimica et Biophysica Acta.***)
2. Nishimura H., Nomura Y., Iwata E., **Sato N.**, and Sako Y. Purification and characterization of carbon monoxide dehydrogenate from the aerobic hyperthermophilic arch eon *Aeropyrum premix*. ***Fisheries Science***, 76:999-1006 (2010).
3. Nishimura H., **Sato N.**, Nomura Y., Iwata E., and Sako Y. Genetic diversity and expression of carbon monoxide dehydrogenate from *Aeropyrum premix*. ***Fisheries Science***, 77:135-141 (2011).